Neutron Scattering in the Analysis of Polymers

C. Michael Roland
Naval Research Laboratory, Washington, DC, USA

1 Introduction **1**
2 Basic Concepts of Neutron Scattering **2**
3 Analysis of Small-Angle Neutron Scattering from Polymers **5**
3.1 Single-Phase Systems 5
3.2 Multicomponent Materials 6
3.3 Small-angle Neutron Scattering and Molecular Motions 8
4 Elastic Small-Angle Neutron Scattering Applied to Polymeric Materials **8**
4.1 Determination of Molecular Parameters 9
4.2 Phase-separated Materials 12
4.3 Effect of Strain and Rheo-small-angle Neutron Scattering 13
4.4 Neutron Reflection 16
4.5 Polymer Dynamics 20
5 Summary **21**
Acknowledgments **22**
Abbreviations and Acronyms **22**
Related Articles **22**
References **22**
Further Reading **27**

The focus of this article is the application of neutron scattering in polymer science, with various examples given to illustrate the types of problems addressed. Neutron scattering is a powerful analytical tool for investigating polymers. Unique aspects such as the capacity to measure thick samples with an absence heating or radiation-induced damage, selective control of the scattering contrast by isotopic substitution, and the measurement of dynamic properties as a function of length scale are among the many attributes that make neutron methods not just complementary to other analytical techniques, but in many cases the only means to address material issues. The information that can be obtained from neutron scattering – the size, form, and orientation of molecular chains, the thermodynamics and phase structure of mixtures, interfaces and interfacial phenomena, the dynamics at both the local and global length scales, details of the structure of complex nanocomposites and biological materials, etc. – has only been surveyed herein. It is a testament to the utility of neutron scattering that even though the application of neutrons to polymers did not begin in earnest until the 1990s, through the past decade, about 325 peer-reviewed publications per year have appeared on the topic. Whether this figure changes in the future will likely depend on the availability of the specialized, costly facilities required for neutron experiments. Certainly there is no expectation of abatement in the number of important problems in polymer science that can be addressed using neutron methods.

1 INTRODUCTION

Neutrons are subatomic particles that stabilize the nuclei of atoms against the electromagnetic repulsions between protons. Impingement on atoms changes the direction of neutrons, and the measurement of the scattering pattern reveals the relative positions of the atoms. Neutrons can also exchange energy with target nuclei, and analysis of this exchange provides information on motions of the atoms. Thus, neutron scattering probes both the structure and dynamics of materials, making the experiments a unique scientific and technological resource. Advantages of neutron scattering experiments include

- Neutrons lack an electric charge and are nonionizing. Their weak interaction with matter makes them very penetrating, and thermal neutrons cause negligible radiation damage. In combination with a lack of sample heating, this makes neutrons well suited for investigation of thick (macroscopic) samples. Also, many materials used in the construction of cryostats, sample cells, etc. are transparent to neutrons.
- Small-angle neutron scattering (SANS) uses neutrons having wavelengths of the order of 10^{-10} m (5–20 Å), which correspond to thermal neutrons with energies in the 5 to 100 meV range ($\approx k_B T$, where k_B is the Boltzmann constant). The wavelength is comparable to interatomic spacing, so that scattering at small angles reveals structural information on length scales of interest to chemists. The broad dynamic range allows the study of molecular rotations, vibrations, and translations and is especially useful for polymers, whose motions span many decades of frequency.
- The interaction (absorption and scattering) of neutrons by elements varies in no systematic fashion across the periodic table, and likewise among isotopes (e.g. hydrogen and deuterium); thus, labeling and

Update based on the original article by D. G. Bucknall, *Encyclopedia of Analytical Chemistry*, © 2000, John Wiley & Sons, Ltd.

Encyclopedia of Analytical Chemistry, Online © 2006–2012 John Wiley & Sons, Ltd.
This article is © 2012 John Wiley & Sons, Ltd.
This article was published in the *Encyclopedia of Analytical Chemistry* in 2012 by John Wiley & Sons, Ltd.
DOI: 10.1002/9780470027318.a2022.pub2

selective probing are extremely useful with SANS through control of the scattering contrast.
- Neutron scattering is sufficiently weak that multiple scattering effects are avoided. And unlike IR and Raman spectroscopies, there are no selection rules restricting the allowed transitions in neutron scattering.

Disadvantages are:

- SANS instrumentation requires dedicated facilities. The neutron sources are expensive to build, operate, and maintain. Small-angle X-ray scattering (SAXS) instruments, in comparison, are relatively low cost and common in individual laboratories.
- The intensity (neutron flux) is lower than that for X-rays, and consequently measurement times tend to be long, and it often requires large amounts of sample (which can be a particular problem for biological investigations).
- The incoherent scattering cross-section for ^{1}H is large and can contribute an unwanted background signal that interferes with analysis of coherent SANS data.

Neutron and X-ray scattering for structural studies cover comparable spatial ranges; however, there are important differences between the methods. While X-rays interact with the electron cloud external to the nucleus, neutrons are scattered by the nucleus (or for polarized neutrons by the magnetic moment of unpaired electrons). The strength of the neutron–nucleus interaction is quantified by the scattering length, b, a property that, as stated, varies randomly across the periodic table and can differ between isotopes of the same element. In particular, deuteration of a compound can effect large changes in contrast, due to the substantial difference in scattering length between hydrogen, $b = -3.739 \times 10^{-13}$ cm, and deuterium, $b = +6.671 \times 10^{-13}$ cm. The contrast in a SANS measurement depends on the squared difference in scattering lengths (Equation 3), which means that large differences in scattering can be achieved between portions of a molecule or among different components of a sample. This property is exploited in many neutron studies.

Neutrons for SANS are produced either as a continuous flux from a nuclear reactor or pulsed, usually from a spallation source. A moderator is used to slow the neutrons to thermal velocities (<10 km s^{-1}), enhancing the resolution. The reactor output is filtered to monochromatize and remove γ-rays, and the beam is also collimated. Spallation sources use a particle accelerator to produce a beam, typically protons, which displaces neutrons from a target of heavy nuclei (^{183}W or ^{238}U). Higher neutron fluxes are achieved, and even when operating in a pulsed mode, the continuous neutron output is about two orders of magnitude higher than that from reactors. The newer neutron sources tend to use particle accelerators. Detectors for neutron scattering are usually two-dimensional (2-D) area detectors. ^{3}He gas is the common active medium, with the incident neutron causing a reaction that forms a proton and a triton. These charged particles are attracted to an anode, with the detected electrical signal proportional to the charge originating with the neutron/^{3}He reaction.

Although neutron scattering experiments require access to a neutron research facility (there are about 30 worldwide), a vast literature has accumulated describing neutron scattering studies of polymers, colloids, metals, glasses, ceramics, biological materials, magnetic solids, superconductors, etc. Herein, the focus is the application of neutron scattering in polymer science, with examples given to illustrate the types of problems addressed; suggestions for further reading are provided at the end.

2 BASIC CONCEPTS OF NEUTRON SCATTERING

The basic neutron scattering experiment is shown in Figure 1. Neutrons from the incident beam interact with the sample and are either blocked by a beam stop

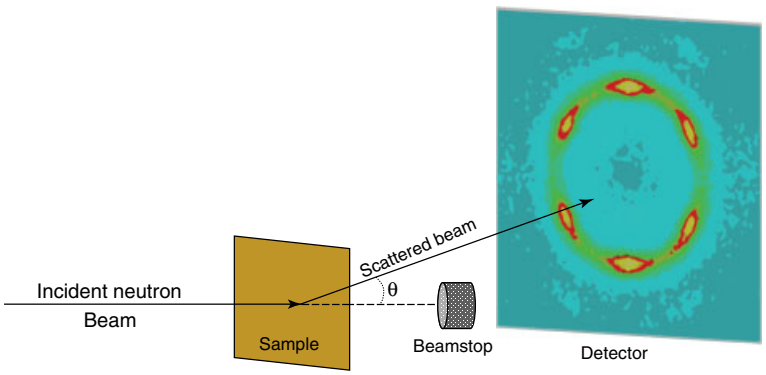

Figure 1 Depiction of typical elastic SANS experiment.

Encyclopedia of Analytical Chemistry, Online © 2006–2012 John Wiley & Sons, Ltd.
This article is © 2012 John Wiley & Sons, Ltd.
This article was published in the *Encyclopedia of Analytical Chemistry* in 2012 by John Wiley & Sons, Ltd.
DOI: 10.1002/9780470027318.a2022.pub2

or scattered onto the detector. The scattered neutrons can change both their energy, E, and direction, the latter expressed as the modulus of the scattering vector, $|Q| = 4\pi/\lambda \sin \theta/2$, where λ is the neutron wavelength and θ the scattering angle. Q (also designated as q, h, k, and s) is sometimes referred to as the momentum transfer, because it is proportional to the change in momentum of the scattered neutron. Elastic scattering implies no energy change ($\Delta E = 0$), and thus only spatial information is provided on the scattering system. Inelastic scattering involves energy exchange due to motion of the scattering nuclei; these measurements can yield information about the dynamics. Commonly, inelastic scattering experiments are termed 'quasielastic', in reference to the small energy change compared with the incident energy. Neutron energies for scattering experiments are a few meV, several orders of magnitude less than the energy of an X-ray photon. The neutron energy is also small compared with the energies associated with vibrational motion, with vibrational scattering peaks present in the spectra approximately equidistance from the elastic peak. Energy differences for rotational and translational motion are small compared with the neutron energy, and thus exchange is manifested as a broadening of the elastic peak.

Two less common applications of neutron scattering are ultra-small-angle neutron scattering (USANS) and wide-angle neutron scattering (WANS). While conventional SANS experiments rely on pinhole collimation and a beam stop to obtain angular resolution, USANS uses a Bonse–Hart camera,[1] in which the incident and scattered beams are reflected multiple times through silicon crystals, precision-cut to maintain parallelism of the refracting planes.[2–4] The minimum angle accessible with USANS is about two decades smaller than that in a SANS experiment, thus overlapping with light scattering methods. For WANS, Q can extend to tens of Å, covering atomic distances. The method is analogous to wide-angle X-ray diffraction measurements; however, isotopic substitution can be employed with WANS to obtain, for example, radial distribution functions for chemically distinct hydrogens in a substance[5] or to circumvent selection rules by breaking the symmetry of the chemical structure.[6]

A measure of the scattering power of a sample is the differential scattering cross-section, $d\Sigma/d\Gamma$, which is the ratio of incident neutrons scatterer per unit time into the solid angle $\Delta\Gamma$. This cross-section is the sum of an angle-independent incoherent component, due to scattering from uncorrelated nuclei, and the coherent scattering. The former is used for inelastic measurements probing molecular motions; however, only the coherent scattering contains the phase information necessary to provide structural information (size and shape of the scattering entities). Integration over all energies and angles gives the total scattering cross-section, which is the sum of the probabilities for neutron scattering with any energy change at all angles. Counting only the number of scattered neutrons regardless of energy,

$$\frac{d\Sigma}{d\Omega} = \int_0^\infty \frac{d^2\Sigma}{d\Omega dE} dE \tag{1}$$

The measured intensity in the absence of multiple scattering is

$$I(Q) = I_0 \Delta\Omega \varepsilon_{det} V \hat{T} \frac{d\Sigma(Q)}{d\Omega} \tag{2}$$

where I_0 is the incident neutron flux, ε_{det} the detector efficiency, and V and $\hat{T}$ are the sample volume and transmission. V, the product of the sample length and the area of the incident beam, is typically in the range from 0.01 to 5 cm^3. When the scattering is dominated by the coherent intensity, $\hat{T}$ must be large (>99%) to avoid multiple scattering, which would distort the measured angle dependence. However, if the incident beam is attenuated due to strong incoherent scattering or absorption, than the optimal coherent intensity is achieved for $T = 37\%$. Standard scatterers can be used to convert the measured data to absolute intensities.

This coherent cross-section is related to properties of the material according to

$$\left.\frac{d\Sigma(Q)}{d\Omega}\right|_{coh} = \phi \Delta\hat{\rho}^2 V_P P(Q) S(Q) \tag{3}$$

where ϕ is the volume fraction of scatterers within the sample, each having a volume V_p. The squared difference between scattering length densities, $\Delta\hat{\rho}^2 = (\hat{\rho}_2 - \hat{\rho}_1)^2$, for two regions or phases in a sample is referred to as the contrast. The scattering length density for a molecule is the sum over all atoms $\hat{\rho} = \sum b_i \rho_i N_A / M_w$, where ρ_i is the mass density, N_A is Avogadro's number, and M_w is the molecular weight.

Listed in Table 1 are scattering length densities for common polymers and solvents. As noted earlier, a distinctive feature of neutron scattering is the contrast between different elements and isotopes, so that the contrast can be adjusted by deuteration or judicious selection of a solvent. However, because the C-D bond distance is a few tenths of a percent smaller than that for C-H bonds (due to a smaller vibrational amplitude), the molecular polarizability is altered by isotopic substitution. This changes the interaction energy and thus in some cases the phase behavior of polymer blends.[7–10] Isotopic polymer mixtures have proven to be very useful in assessing the widely used Flory–Huggins

Encyclopedia of Analytical Chemistry, Online © 2006–2012 John Wiley & Sons, Ltd.
This article is © 2012 John Wiley & Sons, Ltd.
This article was published in the *Encyclopedia of Analytical Chemistry* in 2012 by John Wiley & Sons, Ltd.
DOI: 10.1002/9780470027318.a2022.pub2

Table 1 Neutron Scattering length densities at room temperature for thermal neutrons ('D' denotes perdeuterated compound)

Compound	$\hat{\rho}$ (10^{10} cm^{-2})	Compound	$\hat{\rho}$ (10^{10} cm^{-2})
Polystyrene	1.44	H_2O	−0.56
D-Polystyrene	6.46	D_2O	6.38
Polyethylene	−0.28	Octane	−0.53
D-Polyethylene	6.78	D-Octane	6.43
Polypropylene	−0.28	Cyclohexane	−0.28
Polyethylene oxide	0.64	D-Cyclohexane	6.70
D-Polyethylene oxide	6.46	Chloroform	2.39
Polypropylene oxide	0.34	D-Chloroform	3.16
Polydimethylsiloxane	0.04	D-Decane	−0.49
D-Polydimethylsiloxane	4.66	Tetracosane	0.39
Polymethylmethacrylate	1.10	D-Tetracosane	7.04
D-Polymethylmethacrylate	7.22	Hexatriacontane	−0.36
1,4-Polybutadiene	0.39	D-Hexatriacontane	7.00
D-1,4-Polybutadiene	6.39	*n*-Decyl-tetraoxyethylene	0.18
1,4-Polyisoprene	0.27	D-*n*-Decyl-tetraoxyethylene	6.86
Polyvinylmethylether	0.35	Benzene	1.18
Cholesterol	0.22	D-Benzene	5.42
Fullerene	7.53	Toluene	0.94
Carbon disulfide	1.24	D-Toluene	5.66
Carbon tetrachloride	2.81	Xylene	0.79
		D-Xylene	6.04

theory,[11] because they lack the structural asymmetries and specific interactions encountered in blends of chemically distinct species. The miscibility of isotopic mixtures extends beyond the range predicted by the Flory–Huggins theory[9]; that is, mixtures of isotopes are not 'simple' mixtures.

The last two factors in Equation (3) determine the angle dependence of the scattering. $P(Q)$ is the single-particle form factor, due to interference of waves scattered by different parts of the same body. (Note in some publications, $F(Q)$ is used rather than $P(Q)$.) Form factors are shown in Figure 2 for some common particle shapes. $S(Q)$ is the structure factor, determined by interference among waves scattered from different loci within the sample. $S(Q)$ tends to unity for small particle concentrations and large scattering angles.

For low concentrations of scatterers, the scattering intensity is governed primarily by the form factor; however, for higher concentrations, interparticle correlations become significant. At least for monodisperse particles, $I(Q)$ can be expressed as the product of $P(Q)$, describing the particle shape, and $S(q)$, describing the particle positions. An example is given in Figure 3.[12]

The spatial range with neutron scattering varies from a few angstroms to as much as $\sim 10^5$ Å for USANS; this broad span makes the technique ideal for studying polymers and blends. Not only can measurements be carried out on blends in the homogeneous one-phase region, but also the kinetics of the phase separation process can be investigated, including information about the resulting morphology and domain sizes.

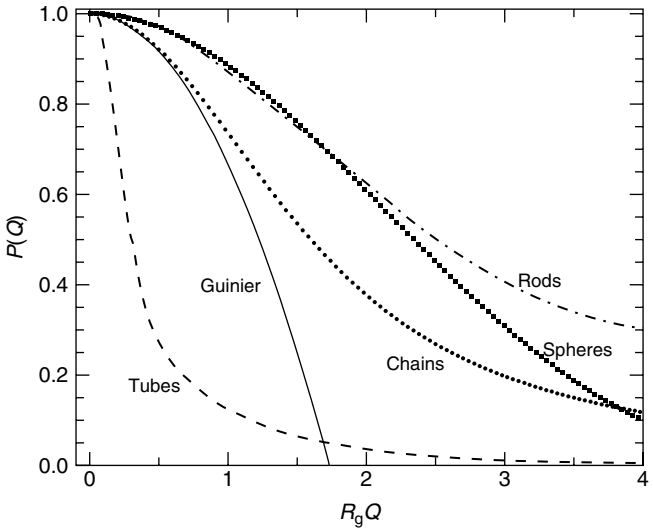

Figure 2 Common form factors for spheres, rods, tubes (i.e. hollow rods), Gaussian chains, and the Guinier approximation (Equation 6) valid at low angles versus the product of the radius of gyration and momentum transfer.

To measure the dynamics of a material, inelastic neutron scattering is employed.[13,14] The techniques include quasielastic neutron scattering (QENS) and neutron spin echo (NSE) experiments. In QENS, time-of-flight or backscattering spectrometers are used. As its name implies, in a time-of-flight experiment, neutrons scattered from the sample are collected as a function of time by wide-angle detectors. Backscattering experiments use a monochromator and analyzer crystals to resolve the

Encyclopedia of Analytical Chemistry, Online © 2006–2012 John Wiley & Sons, Ltd.
This article is © 2012 John Wiley & Sons, Ltd.
This article was published in the *Encyclopedia of Analytical Chemistry* in 2012 by John Wiley & Sons, Ltd.
DOI: 10.1002/9780470027318.a2022.pub2

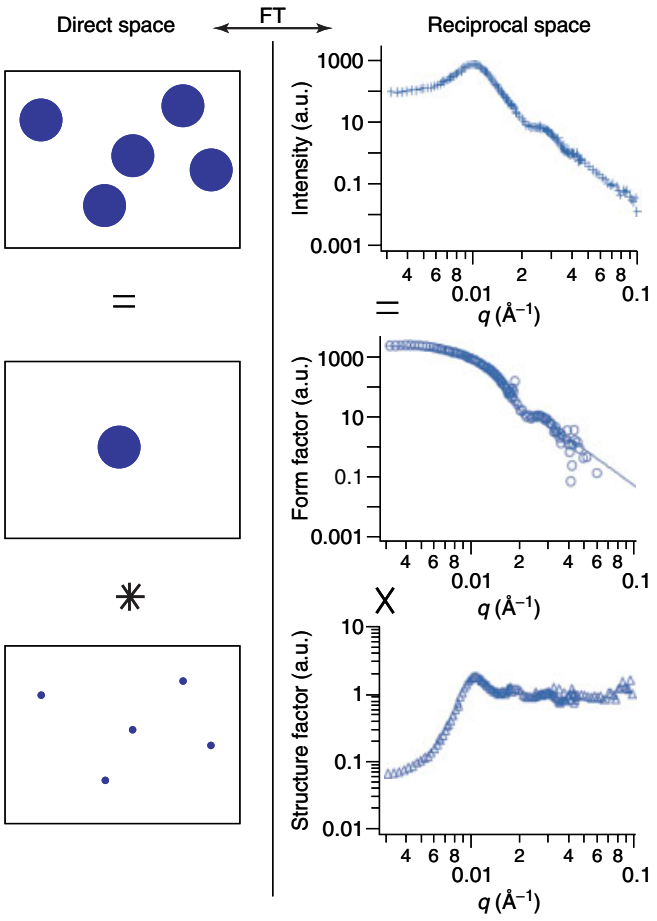

Figure 3 Illustration of particles in direct and reciprocal space. The SANS particle scattering profile is the product of the form factor times the structure factor. The asterisk denotes convolution (from the study by Papon et al.[12] with permission).

energy of the scattered neutrons. NSE experiments take advantage of the magnetic moment of a neutron, which causes its precession at the Lamor frequency when in a magnetic field. This precession functions as an internal clock, providing precise determinations of the energy difference before and after scattering from the changes in neutron polarization with time.

3 ANALYSIS OF SMALL-ANGLE NEUTRON SCATTERING FROM POLYMERS

The distinctive feature of polymer molecules is their range of length scales,[15] and these can be probed in different regions of Q. However, this means that elastic scattering data must be analyzed in a number of ways to extract all the information. Many of the analyses were originally developed for SAXS or light scattering, but can be applied to SANS with minor modifications. Inelastic neutron scattering applied to dynamics is less common in polymer research, although it can be an important supplement to more traditional methods, such as dynamic mechanical and dielectric spectroscopies. The ranges of energy (10^{-8}–1 eV) and momentum transfer (0.1 to ~50 Å^{-1}) for inelastic neutron scattering are very broad, and thus its applicability as a dynamical probe is diverse; for example, molecular vibrations (large ΔE and large Q), rotational tunneling (small ΔE and large Q), aggregate motions in biological systems (small ΔE and small Q), and glassy dynamics (large ΔE and small Q).

3.1 Single-Phase Systems

For a one-phase system, a power series expansion can be used for the form factor:

$$P(Q) = 1 - \frac{R_g^2 Q^2}{3} + \frac{R_g^4 Q^4}{12} - \cdots \tag{4}$$

in which R_g is the radius of gyration. Through the first two terms, this equation is the same as the series expansion of the exponential function; thus, the intensity at small scattering angles can be written as

$$I(Q) \propto \exp\left(-\frac{1}{3} R_g^2 Q^2\right) \tag{5}$$

This is the *Guinier approximation*,[16,17] which provides a model-independent means to determine the radius of gyration of discs, rods, rings, linear and branched macromolecules, etc. For spherical particles, Guinier plots (logarithm of intensity versus Q^2) are linear up to $QR_g < 1$; for elongated particles, the range of validity extends to higher angles (typically $QR_g < 1.3$ for proteins), depending on how the particular shape affects the Q^4 term in Equation (4).

An alternative is the *Zimm approximation*,[18] which incorporates the concentration dependence by making measurements for a number of concentrations and doubly extrapolating to zero concentration and zero Q:

$$\lim_{Q,\varphi \to 0} \frac{\varphi}{I(Q)} = 2A_2\varphi + V_m^{-1}\left(1 + \frac{R_g^2 Q^2}{3}\right) \tag{6}$$

In this equation V_m is the molar volume and A_2 the second virial coefficient characterizing intermolecular interactions. Zimm plots are usually linear over a larger range of Q than the Guinier plot. The intercept of a Zimm plot provides the (absolute) molecular weight, which can serve as a check on the validity of the scattering data. For measurements that do not extend to sufficiently small Q, an alternative 'generalized Zimm plot' has been applied[19,20]:

Encyclopedia of Analytical Chemistry, Online © 2006–2012 John Wiley & Sons, Ltd.
This article is © 2012 John Wiley & Sons, Ltd.
This article was published in the *Encyclopedia of Analytical Chemistry* in 2012 by John Wiley & Sons, Ltd.
DOI: 10.1002/9780470027318.a2022.pub2

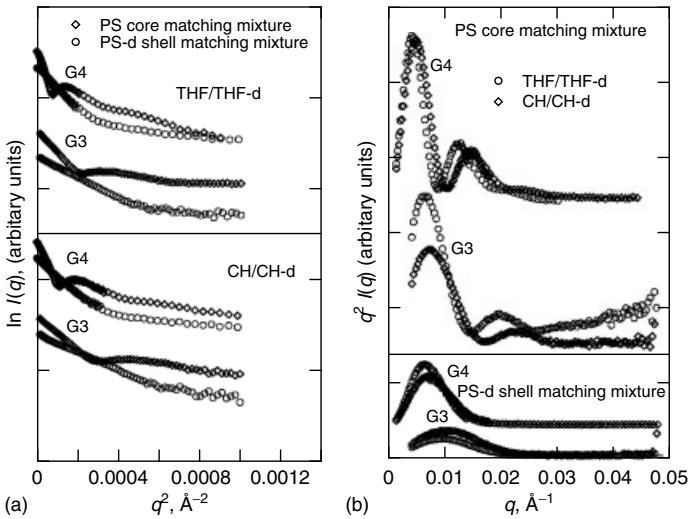

Figure 4 (a) Guinier plots and (b) Kratky plots for SANS data on two arborescent polystyrenes. Different solvents were used to selectively contrast match the inner or outer portions of the molecule, to obtain R_g for the shell and core, respectively. The two methods of analyzing SANS data gave equivalent results (from the study by Yun[23] with permission).

$$I(Q) = \frac{\varphi(1-\varphi)}{[V_m P(Q)]^{-1} + 2A_2\varphi} \tag{7}$$

Scattering data from several concentrations are simultaneously fit to Equation (7), with a model function used for the form factor $P(Q)$.

For Gaussian chains (flexible, linear macromolecules exhibiting a Gaussian distribution of segment densities), the scattering pattern depends only on the radius of gyration and is described by the *Debye function*[21]

$$P(Q) = \frac{2}{R_g^4 Q^4}[\exp(-R_g^2 Q^2) + R_g^2 Q^2 - 1] \tag{8}$$

By measuring two samples having different levels of isotopic substitution, the single-chain scattering contribution can be obtained without going to the limit of zero concentration. The measured coherent scattering for each sample is normalized by the respective scattering length, to yield the structure factor. For small Q ($QR_g << 1$), Equation (8) is equivalent to Equation (6); for intermediate Q ($QR_g > 1$), Equation (8) gives

$$P(Q) \approx \left(1 + \frac{R_g^2 Q^2}{2}\right)^{-1} \tag{9}$$

Thus, a plot of $I(Q)Q^2$ versus Q [*Kratky plot*[22]] should asymptotically approach a plateau value, which yields the molecular size. This analysis is often applied to determine the conformation of proteins (e.g. their folding). If the polymer has a non-Gaussian distribution of chain lengths, such as for branched or star polymers, the Kratky plot deviates from the plateau. Figure 4 compares Guinier and Kratky plots for arborescent (graft dendritic) polystyrene.[23]

3.2 Multicomponent Materials

According to the random phase approximation (RPA),[11] the coherent SANS intensity due to concentration fluctuations (assuming incompressibility and therefore no density fluctuations) is

$$I(Q)^{-1} = \Delta\rho^{-2}\left[\frac{1}{\varphi_1 v_1 N_1 P_1(Q)} + \frac{1}{\varphi_2 v_2 N_2 P_2(Q)} - \frac{2\chi}{\sqrt{v_1 v_2}}\right] \tag{10}$$

where v is the monomer volume, N_i the degree of polymerization, and the contrast factor is per monomer volume. $P(Q)$ in Equation (10) is the single-chain scattering function (Equation 8); thus, the RPA expresses the structure factor of a system of interacting chains in terms of those of a noninteracting ('ideal') system. Equation (10) enables determination of the interaction parameter, χ, which is a measure of the mixing enthalpy plus any noncombinatorial entropy contributions to the free energy (the latter arising, for example, from equation of state effects due to size differences between components). Reflecting limitations of the RPA description, experimentally χ is not strictly constant, but can depend on temperature, molecular weight, composition, and even on Q.[24–26] An example of the application of the RPA equation to a polymer blend is shown in Figure 5.[27] The data are plotted in the

Encyclopedia of Analytical Chemistry, Online © 2006–2012 John Wiley & Sons, Ltd.
This article is © 2012 John Wiley & Sons, Ltd.
This article was published in the *Encyclopedia of Analytical Chemistry* in 2012 by John Wiley & Sons, Ltd.
DOI: 10.1002/9780470027318.a2022.pub2

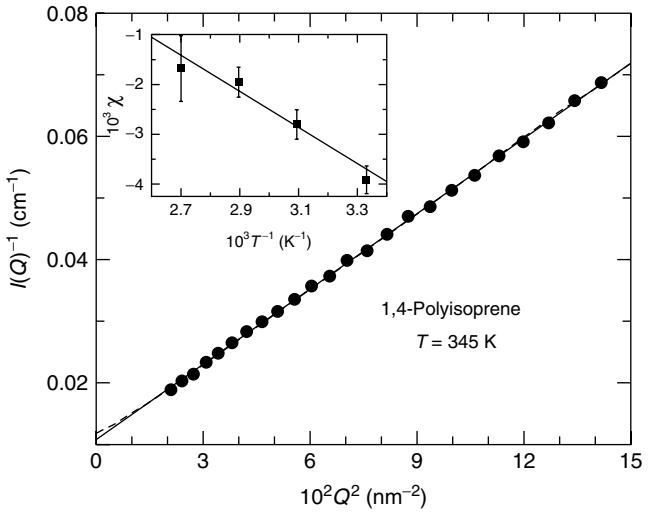

Figure 5 SANS intensity for isotopic mixture plotted in the Ornstein–Zernike form (solid line is linear fit), along with the fit to Equation (10) (dashed line); the difference between the analyses is only apparent at small Q. Inset shows the interaction parameter determined from measurements at four temperatures, yielding $\chi = 8.3 \times 10^{-3} - 3.6/T$ (from the study by Tomlin and Roland[27]).

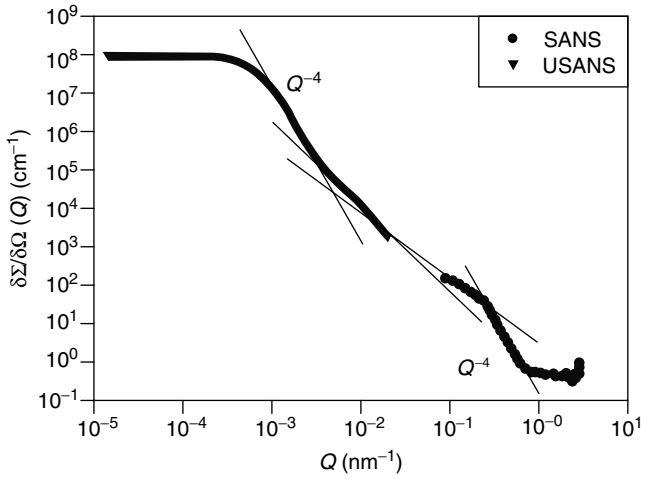

Figure 6 SANS and USANS of a solution of poloxamer triblock copolymer (an amphiphilic polymer commercially known as Pluronic®). The various Q-dependences at different scattering angles are denoted by the solid lines, with two Porod regions (from the study by Sharp et al.[37] with permission).

Ornstein–Zernike form[11]:

$$I(Q)^{-1} = \Delta\rho^{-2}[a_0 + a_1 Q^2] \tag{11}$$

valid at small Q. The intercept of Equation (11) yields the interaction parameter directly.

For a phase-separated material having a random distribution of phases, the length scale of the composition variations, ξ, can be determined from the *Debye–Bueche function*[28]:

$$I(Q) = 8\pi\varphi(1-\varphi)\Delta\rho^2 \frac{\xi^3}{(1+\xi^2Q^2)} \tag{12}$$

A plot of $I(Q)^{-1/2}$ versus Q^2 yields the correlation length in the limit of small Q. Equation (12) can be applied to high concentrations, where the domains are mutually correlated.[29,30] This differs from the Guinier analysis (Equation 5) for isolated domains. The high resolution of SANS, especially USANS, makes the technique more useful than SAXS for studying the large domains often encountered with polymeric materials.[31–35]

In the case of sharp boundaries, the coherent scattering at higher angles has a Q^{-4} dependence in accord with *Porod's law*[36]:

$$I(Q) = 2\pi\Delta\rho^2\hat{S}Q^{-4} \tag{13}$$

where $\hat{S}$ is the surface area to volume ratio. Rough or diffuse interfaces reduce the exponent in Equation (13) to less than 4. Figure 6 shows SANS and USANS data, in which two Porod regions are observed corresponding to scattering from polymer micelles at high Q and agglomerated micelles at smaller Q.[37]

By combining WANS, SANS, and USANS, an enormous span of scattering vectors can be probed. Figure 7 is an example of neutron scattering data combining the three experiments, with various analyses applied to the different Q ranges.[38]

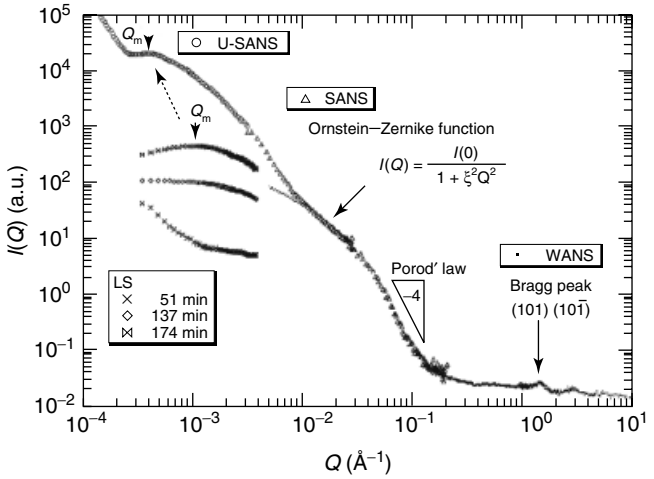

Figure 7 Swollen polyvinyl alcohol gels. Along with the phase-separated domains, the cross-links give rise to crystalline Bragg maxima at $Q = Q_m$ (Kanaya et al.[38] with permission).

Encyclopedia of Analytical Chemistry, Online © 2006–2012 John Wiley & Sons, Ltd.
This article is © 2012 John Wiley & Sons, Ltd.
This article was published in the *Encyclopedia of Analytical Chemistry* in 2012 by John Wiley & Sons, Ltd.
DOI: 10.1002/9780470027318.a2022.pub2

3.3 Small-angle Neutron Scattering and Molecular Motions

Sections 3.1 and 3.2 pertain to elastic experiments, in which there is no energy discrimination of the scattering. However, experiments can also measure the number of neutrons scattered that exchange energy with the sample by an amount dE; this yields the double differential scattering cross-section:

$$\frac{\partial^2 \Sigma}{\partial \Omega \partial E} = \frac{\sigma_{inc}}{4\pi} S_{inc}(Q, \omega) + \frac{\sigma_{coh}}{4\pi} S_{coh}(Q, \omega) \qquad (14)$$

In Equation 14, σ_{inc} and σ_{coh} are the respective incoherent and coherent cross-sections, and $S(Q, \omega)$ are the dynamic structure factors.

The Fourier transform of $S_{inc}(Q, \omega)$ gives the intermediate scattering function, $S_{inc}(Q, t)$, from which the self-part of the van Hove correlation function[39] can be obtained. (The van Hove function gives the probability of finding a particle i at position r at time t when there is a particle j at the origin at time 0; the self-part means i and j are the same particle.) The frequency is given by the Planck relation, $\omega = E/(2\pi h)$. Under the usual condition of small energy changes, Q is close to the corresponding value for elastic scattering, $= 4\pi/\lambda \sin \theta/2$.

Figure 8 shows quasielastic intensities, $I(Q, \omega)$, measured in the frequency domain. The motion of the scattering nuclei causes broadening from the profile of the elastic background.[40] The Fourier transform of these data yield the $I(Q, t)$ shown in Figure 9.[40] The broader peaks, reflecting faster motions, result in a more rapid decay of the correlation of the nuclei positions over time relative to their positions at an initial time 0.

Although experimental methods such as dielectric spectroscopy, dynamic light scattering, mechanical measurements, and nuclear magnetic resonance (NMR) are more prevalent in studies of molecular and polymer dynamics, neutron scattering methods offer certain advantages. In addition to the ability to enhance and tailor the contrast of the sample constituents, the QENS and NSE methods provide spatial information, because the scattering can be measured as a function of wave vector. The utility of this property is illustrated in a study of methacrylate polymers, in which motion of the pendant group was resolved from the main-chain dynamics by measuring the scattering at different values of Q (Figures 10–12).[41]

QENS and NSE measurements interrogate the dynamics at very short times ($<10^{-8}$ s). For slow processes, the static scattering can be measured as a function of time. However, changes occurring over intermediate timescales are more difficult to monitor with SANS. One approach is to resolve the output of the 2-D positional detector over time, which allows dynamic data to be obtained for processes having time constants on the order of 0.1 s.[42]

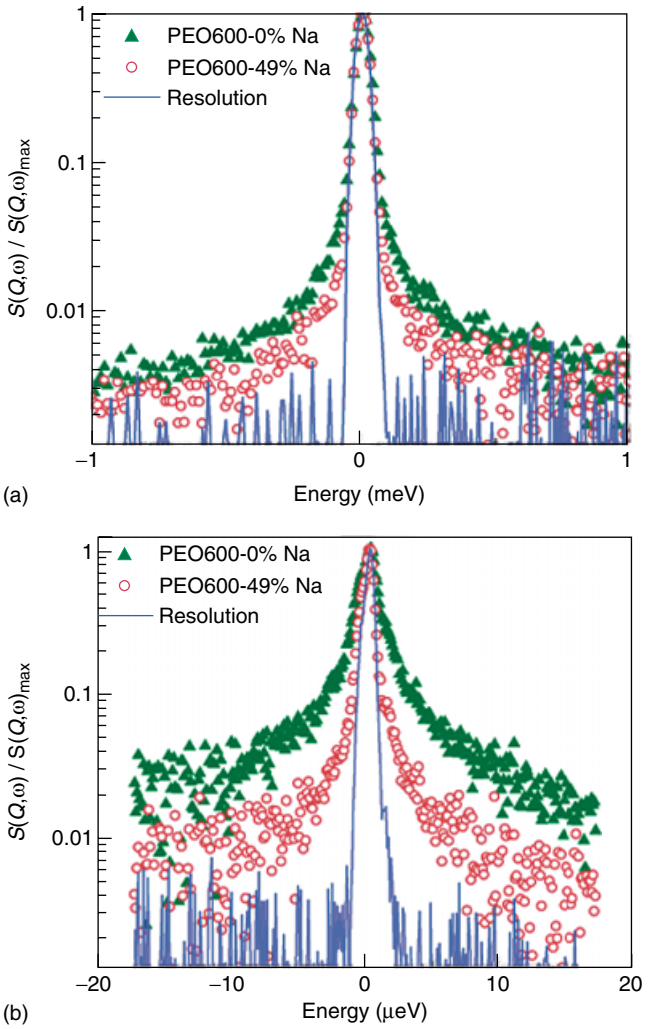

Figure 8 Frequency domain QENS data from two spectrometers: (a) 0.4–50 ps temporal range; (B) 250–2500 ps range, both at $Q = 1.04\,\text{Å}^{-1}$. The sample was a polyethylene oxide conducting polymer with 0% (filled symbols) and 4% (hollow symbols) ion content. The presence of ions reduces the chain mobility (from the study by Sinha and Maranas[40] with permission).

4 ELASTIC SMALL-ANGLE NEUTRON SCATTERING APPLIED TO POLYMERIC MATERIALS

Analysis of the angle dependence of neutron scattering provides structural and morphological information, and there is an enormous literature describing the application of SANS to polymeric materials. Selected aspects are described later to illustrate the broad utility of the technique.

Encyclopedia of Analytical Chemistry, Online © 2006–2012 John Wiley & Sons, Ltd.
This article is © 2012 John Wiley & Sons, Ltd.
This article was published in the *Encyclopedia of Analytical Chemistry* in 2012 by John Wiley & Sons, Ltd.
DOI: 10.1002/9780470027318.a2022.pub2

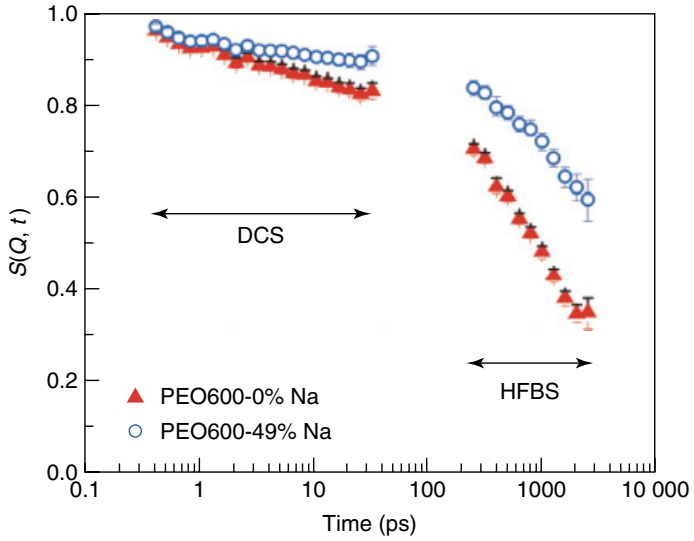

Figure 9 Inverse Fourier transformed data from Figure 8. The faster segment motion in PEO lacking added ions (filled symbols) causes a more rapid decay of the self-intermediate scattering function (from the study by Sinha and Maranas[40] with permission).

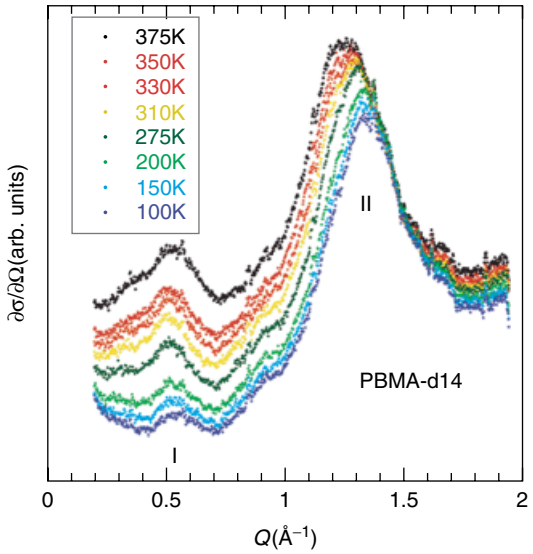

Figure 10 Differential scattering cross-sections measured for deuterated polybutylmethacrylate. The two peaks at $Q \approx 0.5$ and 1.3 $Å^{-1}$ correspond to correlations between units in the main chain and between atoms located in side groups, respectively (from the study by Arbe et al.[41] with permission).

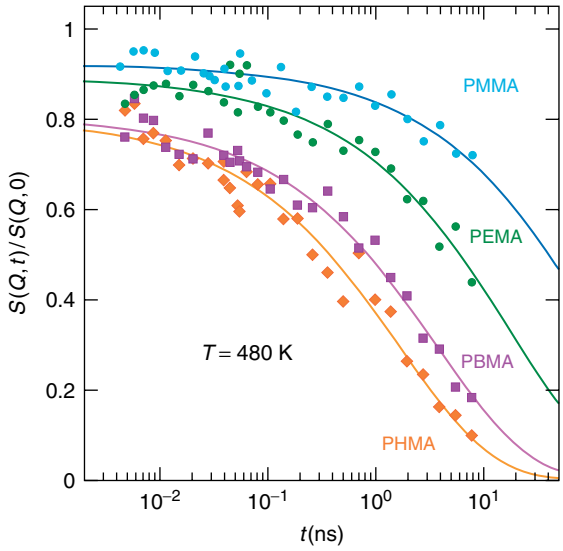

Figure 11 Dynamic structure factor for methacrylate polymers with different side groups, measured at the maximum at lower angle (peak I at 0.5 $Å^{-1}$ in Figure 10). The dynamics correspond to structural relaxation of the main chain (from the study by Arbe et al.[41] with permission).

4.1 Determination of Molecular Parameters

The scattering at large Q reflects the short-range, intramolecular correlations of the polymer segments. As shown from scattering measured for polybutadiene at three temperatures spanning the glass transition (Figure 13[43]), the static structure factor for $Q > 5\,Å^{-1}$ remains constant. However, glass formation affects the position and intensity of peaks at small values of Q ($<2.5\,Å^{-1}$), due to the significant change in molar volume (thermal expansivity) altering intermolecular correlations.

As seen from the equations in Sections 3.1 and 3.2, detailed analysis of the Q dependence of SANS can yield information on the polymer chain conformation and also the interaction parameter of mixtures. Using the Guinier (Equation 5), Debye (Equation 8), or RPA (Equation 10) equations, the radius of gyration of the polymer can be calculated (as seen in Figure 2, the scattering function for a Gaussian coil depends only on

Encyclopedia of Analytical Chemistry, Online © 2006–2012 John Wiley & Sons, Ltd.
This article is © 2012 John Wiley & Sons, Ltd.
This article was published in the *Encyclopedia of Analytical Chemistry* in 2012 by John Wiley & Sons, Ltd.
DOI: 10.1002/9780470027318.a2022.pub2

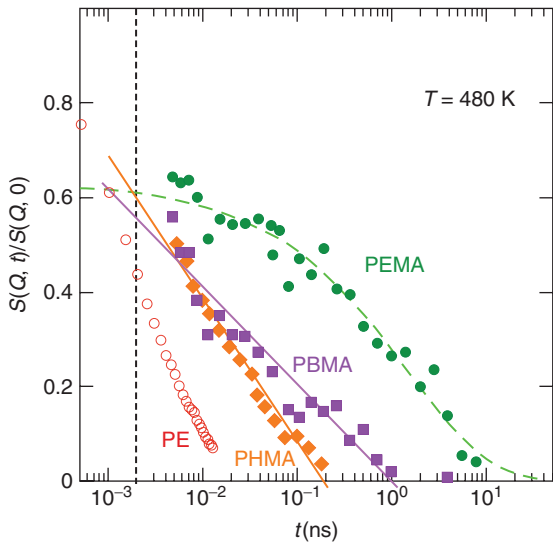

Figure 12 Comparison of the dynamic structure factors at the higher angle maximum (peak II at 1.3 Å^{-1} in Figure 10), for three methacrylate polymers (filled symbols) and a polyethylene (open circles). The NSE behavior reflects structural relaxation of the side groups (from the study by Arbe et al.[41] with permission).

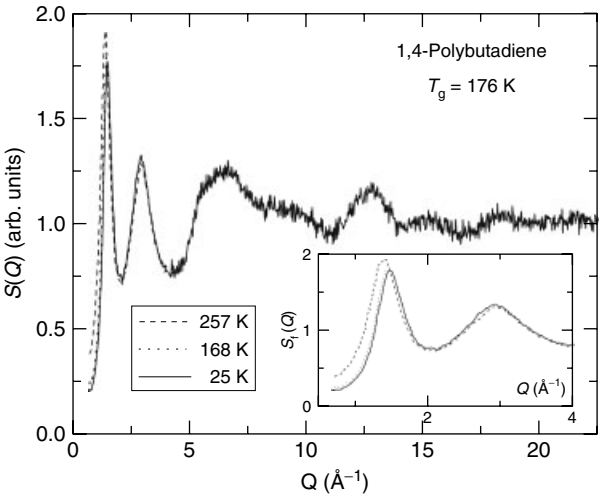

Figure 13 Static structure factor from SANS for polybutadiene measured in the liquid state (dashed line), just below T_g (dotted line), and deeply in the glassy state (solid line). The small Q scattering is shown on an expanded scale in the inset (data from the study by Frick et al.[43]).

the radius of gyration). The single-chain structure factor for polyisoprene extracted from SANS measurements on two samples differing in deuteration level is shown in Figure 14.[44] The fit to Equation (8) yields $R_g = 34$ Å. Applying Equation (5) to the same data in the limit of zero Q yields $R_g = 31$ Å.

The branch structure of polymers is difficult to quantify by conventional methods; however, the results from scattering experiments to characterize the chain size can be combined with NMR or other spectroscopic determinations of (number average) branch concentration to obtain detailed information, especially when measurements are made on various molecular weight fractions. Figure 15[45] shows the persistence length, l_p, from SANS

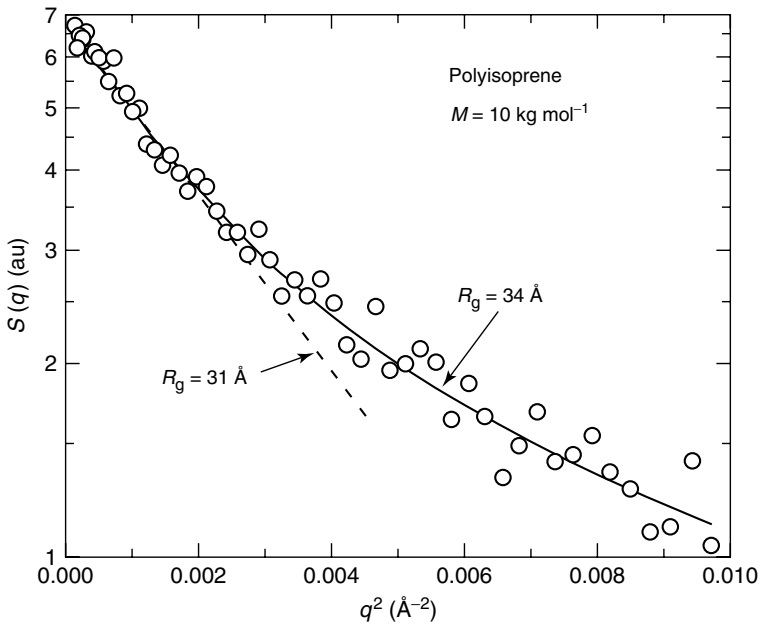

Figure 14 Single-chain structure factor for a blend of deuterated and normal polyisoprene, plotted in the Guinier form. The solid line is the fit to the Debye equation, and the dashed line the Guinier fit to the low Q data (from the study by Akcasu et al.[44]).

Encyclopedia of Analytical Chemistry, Online © 2006–2012 John Wiley & Sons, Ltd.
This article is © 2012 John Wiley & Sons, Ltd.
This article was published in the *Encyclopedia of Analytical Chemistry* in 2012 by John Wiley & Sons, Ltd.
DOI: 10.1002/9780470027318.a2022.pub2

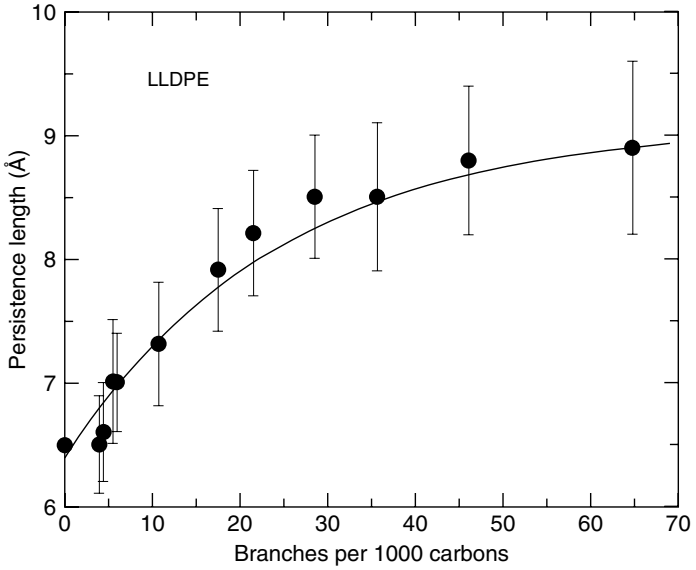

Figure 15 Persistence length of linear low-density polyethylene chains versus the number of butyl branches. The line is the fit of Equation (15) (data from the study by Ramachandran et al.[46]).

plotted as a function of the number of branches per thousand carbon atoms (determined from NMR). The data are fit to an empirical expression relating l_p to the number branches[46]:

$$l_p = l_p^{\infty} - k_1 \exp(-n/k_2) \tag{15}$$

in which l_p^{∞} is the persistence length for complete branching, and k_1 and k_2 are constants, the former specific to the polymer and the latter depending on the type of branches. For polyethylene, $l_p^{\infty} = 9.1 \pm 0.4$ Å.[46]

The formation of polymethymethacrylate (PMMA) star polymers by linking linear chains was followed by in situ SANS measurements carried out as a function of reaction time.[47] As shown in Figure 16, the time evolution of characteristic structural parameters can be extracted from analysis of the scattering profiles.

SANS is commonly used to study phase behavior and the morphology of block copolymers and blends.[48,49] In principle, both density and composition fluctuations contribute to the small-angle scattering. By selective isotopic labeling of the components, the two effects can be characterized independently. This is illustrated in Figure 17 for a blend of polyethylene oxide (PEO) and PMMA.[50] As the PEO is deuterated, the scattering is mainly from composition fluctuations, which increase with temperature as the LCST (lower critical solution temperature) is approached. The scattering due to density fluctuations, determined by measurement on a completely protonated sample, is indicated in the figure.

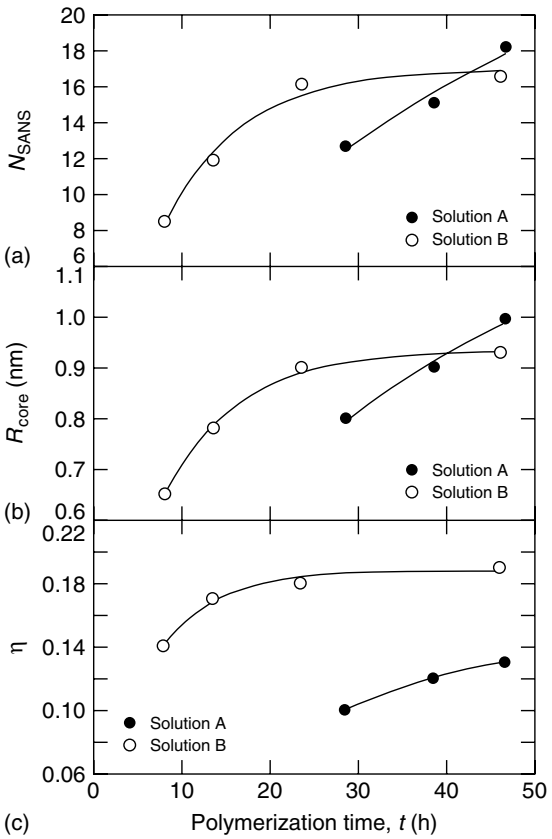

Figure 16 (a) Number of arms per molecule, (b) radius of the core, and (c) volume fraction of the equivalent hard spheres for PMMA star polymers, as determined from time-resolved SANS profiles of the reaction solution (from the study by Terashima et al.[47] with permission).

Encyclopedia of Analytical Chemistry, Online © 2006–2012 John Wiley & Sons, Ltd.
This article is © 2012 John Wiley & Sons, Ltd.
This article was published in the *Encyclopedia of Analytical Chemistry* in 2012 by John Wiley & Sons, Ltd.
DOI: 10.1002/9780470027318.a2022.pub2

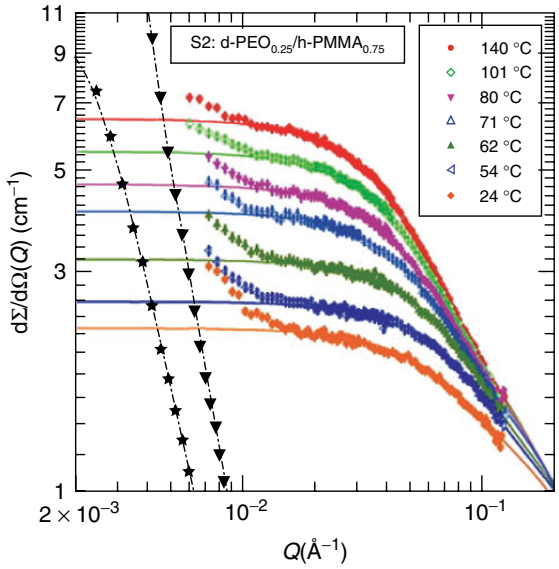

Figure 17 SANS from a blend of deuterated polyethylene oxide and protonated polymethylmethacrylate. The upturn at low Q is due to density fluctuations, whose contribution was determined from SANS on blends without isotopic contrast (and indicated by the scattering data below $Q \approx 10^{-2}$ Å^{-1}). Note the Ornstein–Zernicke Q^{-2} dependence at high Q (Equation 11) (from the study by Schwahn et al.[50] with permission).

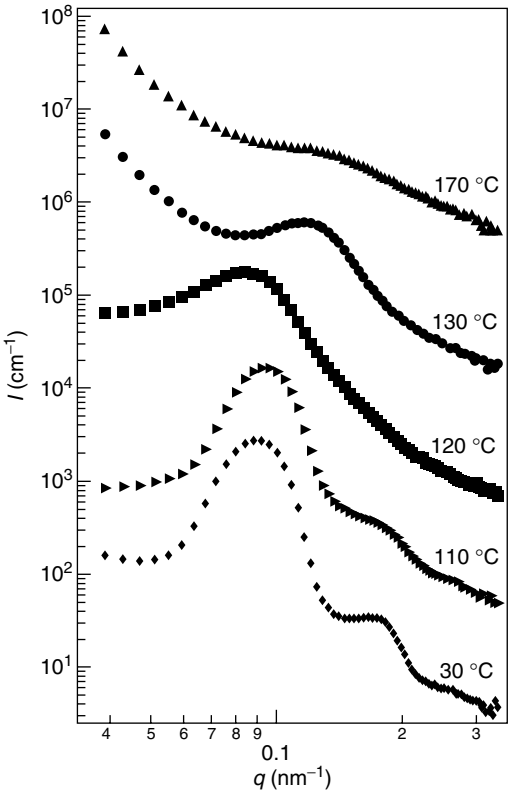

Figure 18 SANS intensity of a blend of saturated 1,2-polybutadiene and polyisobutylene with added diblock copolymer as a compatibilizer. At temperatures below the critical temperature, 120 °C, the lamellar structure gives rise to peaks at Q_m and $2Q_m$. At higher temperatures, the morphology becomes homogeneous and the peaks are absent (from the study by Nedoma et al.[51] with permission).

4.2 Phase-separated Materials

The phase separation process can be followed using SANS, with nucleation and growth versus spinodal decomposition mechanisms easily distinguished (Figure 18[51]). The phase separation process in polymers is slow enough that time-resolved scattering experiments can be performed. For spinodal decomposition, the length scale, l_m, of the phase-separated morphology produces a maximum in the scattering curve at a scattering angle given by the Bragg formula, $Q_m = 2\pi/l_m$. If the phase separation proceeds by nucleation and growth of domains, the morphology is too irregular to yield such maxima, although there is an increase in the scattering intensity ('cloud point'). This can be assessed from the scattering invariant:

$$\hat{I} = \int_0^\infty Q^2 \frac{d\Sigma}{d\Omega}(Q) dQ \qquad (16)$$

In calculation of scattering invariants, the integration extends only to angles for which there is measurable intensity in the background-corrected scattering; however, for a two-phase system, this scattering at high Q usually makes a negligible contribution to $\hat{I}$.

Block copolymers, in which the chain molecules comprise multiple sequences of repeat units, are an important class of materials with widespread commercial applications. When the blocks are thermodynamically immiscible, phase segregation occurs, giving rise to morphologies ranging from spherical, cylindrical, gyroid, or lamellar, as governed by the block lengths and matrix.[52–55] SANS has been applied extensively to investigate the morphology of block copolymers. In Figure 19 are SANS data for styrene–isoprene diblock copolymer in which the styrene was fully deuterated. Peaks corresponding to successive orders in the interference pattern are evident.[56]

Figure 20 compares the SANS and SAXS patterns from a triblock polymer.[57] The diffraction intensities are calculated from the Fourier coefficients of the segment densities, each term corresponding to a particular reflection.[58]

The distribution of deuterated water in epoxy hydrogels was studied using SANS.[59] Two regimes for the morphology were observed: below the percolation threshold of water, isolated water-rich domains are dispersed in a continuous water-poor epoxy matrix; at higher water content, these domains become continuous. With continuity of the dispersed phase, there is a diminution of the scattering maxima (Figure 21).

Encyclopedia of Analytical Chemistry, Online © 2006–2012 John Wiley & Sons, Ltd.
This article is © 2012 John Wiley & Sons, Ltd.
This article was published in the *Encyclopedia of Analytical Chemistry* in 2012 by John Wiley & Sons, Ltd.
DOI: 10.1002/9780470027318.a2022.pub2

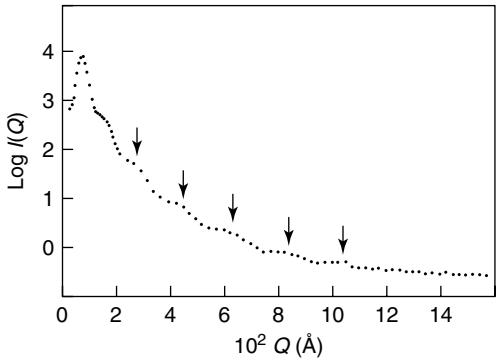

Figure 19 SANS from an isoprene–styrene diblock copolymer. The arrows denote the scattering vectors of the various Bragg diffraction peaks. The most intense at $Q \sim 0.008$ corresponds to a domain spacing of about 800 Å (Richards[56] with permission).

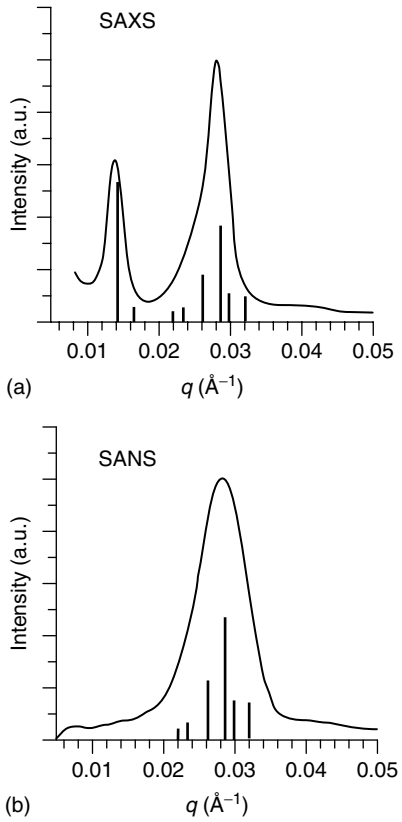

Figure 20 Small-angle X-ray scattering and SANS diffraction patterns from an isoprene–styrene–dimethylsiloxane triblock copolymer. The histogram bars are the calculated intensities of the various peaks assuming a core-shell gyroid morphology. The first-order reflections are cancelled in the SANS spectra (Shefelbine et al.[57] with permission).

Polymer composites, in which filler particles are used to reinforce or otherwise modify the properties, are very common materials. The resolution of SANS and USANS is advantageous for characterizing particles sizes,[60–63] including rheo-SANS experiments that probe the effect of deformation on the particulate structure[12,64–66] (Section 4.3). Chu and Liu[67] compared light, X-ray, and neutron scattering methods for determination of the size of particulate fillers in polymers. Figure 22 shows SANS curves measured for polystyrene/silica nanocomposites.[68] After normalizing the intensity by the filler content, the curves superpose at high angles, with agglomeration of the silica giving rise to a peak at smaller scattering angles, at a value of Q_m that varies with the 0.87 power of the filler volume fraction.

Polyhedral oligomeric silsesquioxane (POSS) is one of the smallest filler particles, with a symmetric, three-dimensional nanostructure. In Figure 23[69] are SANS data for POSS suspended in deuterated toluene.

A study of polyurea ceramic composites using WANS measurements was carried out (Figure 24).[70] The small pore size of the ceramic required the wider angle measurements, which provide information similar to X-ray scattering, but with different contrast.

4.3 Effect of Strain and Rheo-small-angle Neutron Scattering

The ability of SANS measurements to provide structural information makes it useful for investigating the effect of deformation and flow on materials. The greater penetrating power of neutrons is a key advantage of SANS over SAXS or light scattering for such experiments. Also, contrast matching can be employed to probe the orientation or positional ordering of specific components of the sample. For solids or materials with a stable morphology, the scattering can be measured subsequent to the deformation, although in situ measurements made on flowing samples (rheo-SANS) is an increasingly popular technique.

Phase-separated polymeric materials, including gels (cross-linked rubbery polymers in solution), produce characteristic scattering when deformed known as butterfly patterns. These are isointensity contours on a 2-D detector that have a double-winged shape, symmetric along the stretch direction.[48,71–74] Shibayama[75] has reviewed the various butterfly patterns characteristic of different types of gels. An example for a sheared blend is shown in Figure 25.[76]

Figure 26 shows the SANS and SAXS intensities parallel and perpendicular to the orientation direction for drawn polyethylene ($M_w = 2 \times 10^6$ g/mol) containing a few percent of deuterated PE ($M_w = 2 \times 10^5$ g/mol). Using the SAXS data to subtract the contribution from density fluctuations, the resulting scattering patterns were fit to a model to obtain a quantitative description of the shish-kebab, extended chain semicrystalline morphology.[77]

Encyclopedia of Analytical Chemistry, Online © 2006–2012 John Wiley & Sons, Ltd.
This article is © 2012 John Wiley & Sons, Ltd.
This article was published in the *Encyclopedia of Analytical Chemistry* in 2012 by John Wiley & Sons, Ltd.
DOI: 10.1002/9780470027318.a2022.pub2

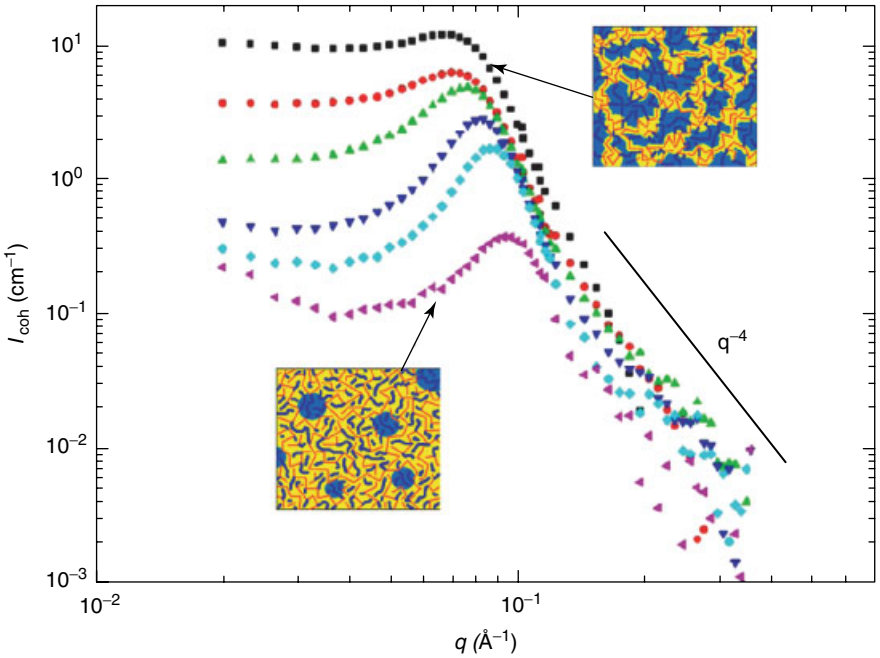

Figure 21 Coherent SANS intensities for swollen epoxy networks (heavy water concentrations by weight = 0%, 23%, 47%, 58%, 67%, 72%, and 77% from bottom to top). Schematics are shown for the structure below and above the concentration for percolation of the water phase (from the study by Krakovsky et al.[59] with permission).

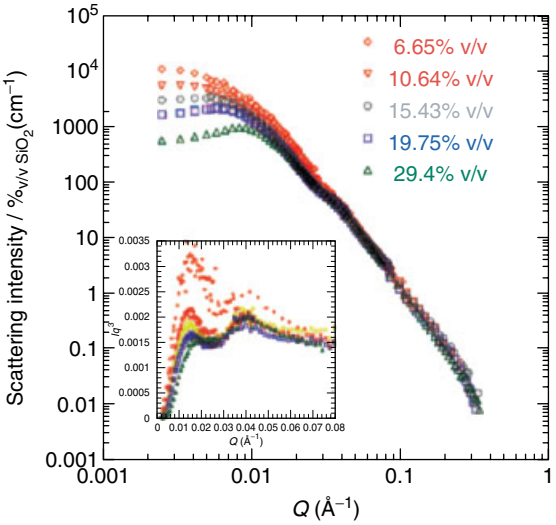

Figure 22 Coherent SANS for PS with differ amounts of silica particles. At high Q, the intensity deceases as Q^{-4}, reflecting the sharp interface between the polymer and the silica (Equation 13). The inset shows the oscillations in IQ^3 in the region around $Q = 0.04$ Å, due to internal structure within the silica aggregates (from the study by Jouault et al.[68] with permission).

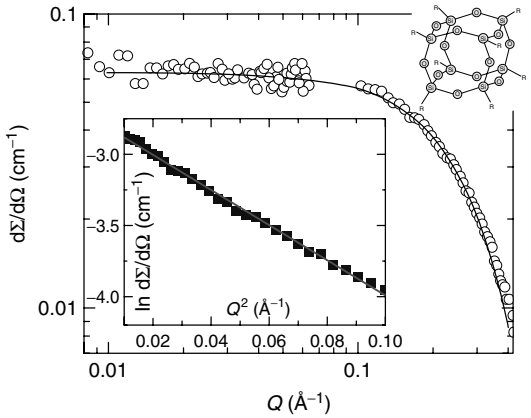

Figure 23 Form factor for POSS particles (structure shown) in dilute toluene solution. Guinier plot in the inset yields $R_g = 6$ Å (from the study by Nusser et al.[69] with permission).

An example of following phase separation by making SANS measurements as a function of time is shown in Figure 27 or a blend of PS and PMMA.[78] Deformation affects the phase separation behavior; thus, the scattering patterns differ after imposition of small and large shear strains. The latter accentuates phase separation, with consequent increase in the scattering intensity and a shift of the maximum to smaller angles.

The opposite of phase segregation, coalescence of dispersed polymer phases, can also be quantified using SANS. Phase-separated blends usually consist of discrete particles in a continuous phase. For an immiscible blend, this globular morphology is never at equilibrium; rather, the size distribution of the dispersed phase is a steady-state balance between the breakup of the particles

Encyclopedia of Analytical Chemistry, Online © 2006–2012 John Wiley & Sons, Ltd.
This article is © 2012 John Wiley & Sons, Ltd.
This article was published in the *Encyclopedia of Analytical Chemistry* in 2012 by John Wiley & Sons, Ltd.
DOI: 10.1002/9780470027318.a2022.pub2

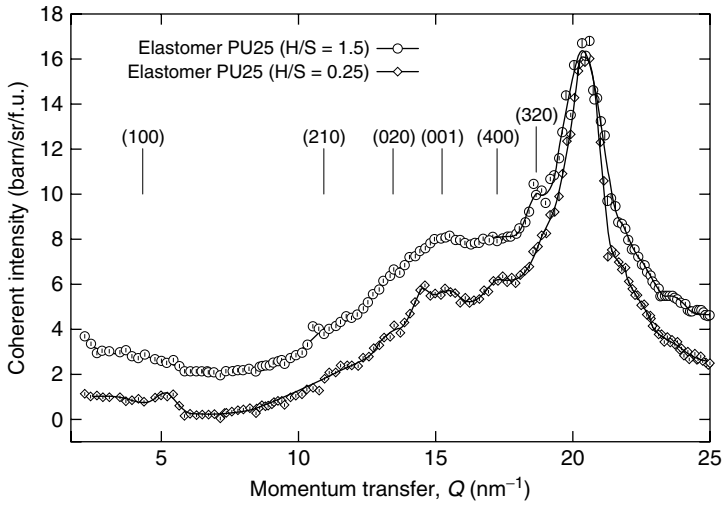

Figure 24 WANS from polyurea polymers synthesized within the pores of a ceramic (the two curves correspond to different ratios of isocyanate to polyamine). The ordering of the hard domains gives rise to crystalline-like reflections, denoted in the figure (from the study by Zaj[1]c et al.[70] with permission).

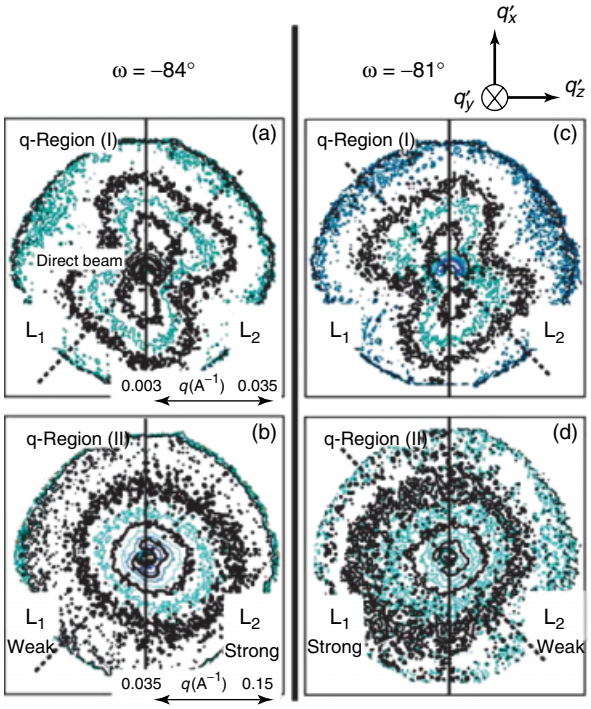

Figure 25 SANS profiles of a blend of polystyrene and polyvinylmethylether for shear rotation of the indicated magnitudes. The upper curves are the low Q range at which a double-lobe pattern is observed. The lower curves at higher scattering angle exhibit an elliptical shape. The directions of shear, velocity gradient, and vorticity are x, y, and z, respectively (from the study by Koizumi and Suzuki[76] with permission).

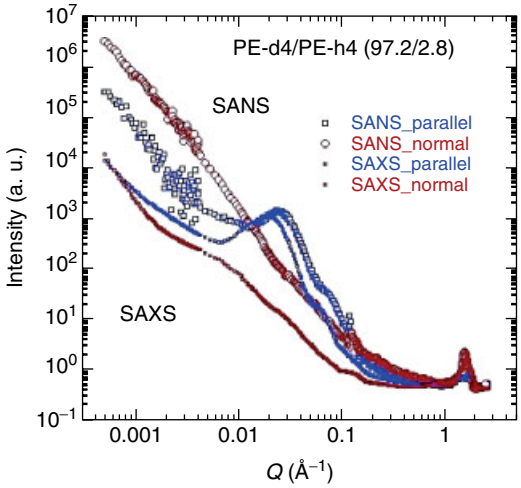

Figure 26 Scattering from high molecular weight polyethylene containing 2.8% deuterated PE measured along and transverse to the elongation direction (Kanaya et al.[77] with permission).

and their coalescence. This flow-induced coalescence was followed for polybutadiene particles dispersed in a polychloroprene matrix from the change in the SANS invariant (Equation 16) with time of shearing (Figure 28).[79] Initially, the particles were either wholly deuterated or protonated polybutadiene; coalescences causes particles to have a mixed isotopic composition, which reduces the scattering intensity.

The rheo-SANS method involves combining flow of the sample with simultaneous scattering measurements.[80] These experiments employ various flow types and geometries, including shear flow in concentric cylinders (Couette cell), sliding plates, or extensional flow using, for example, capillary tubes or flow from opposing jets. The anisotropy of the flow field defines different scattering planes, as illustrated in Figure 29 for a Couette

Encyclopedia of Analytical Chemistry, Online © 2006–2012 John Wiley & Sons, Ltd.
This article is © 2012 John Wiley & Sons, Ltd.
This article was published in the *Encyclopedia of Analytical Chemistry* in 2012 by John Wiley & Sons, Ltd.
DOI: 10.1002/9780470027318.a2022.pub2

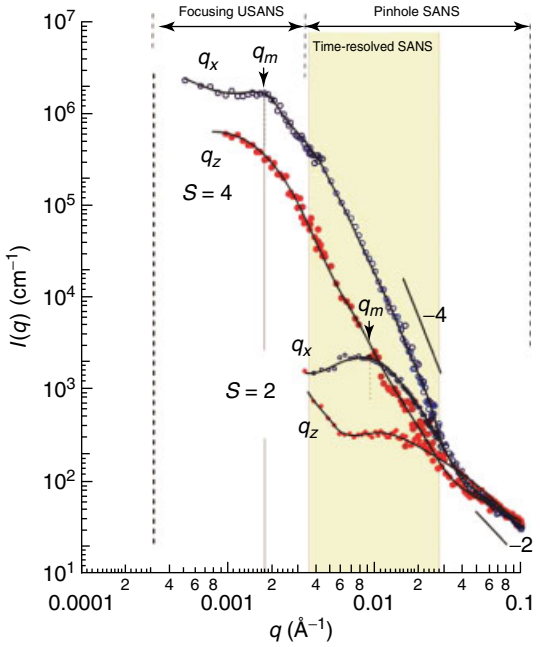

Figure 27 SANS and USANS measured along the shear (x) and vorticity (z) directions following shear-induced phase separation from a blend of PS and PVME (S indicates the value of the shear strain). The scattering at high angle follows Porod's law (from the study by Koizumi and Inoue[78] with permission).

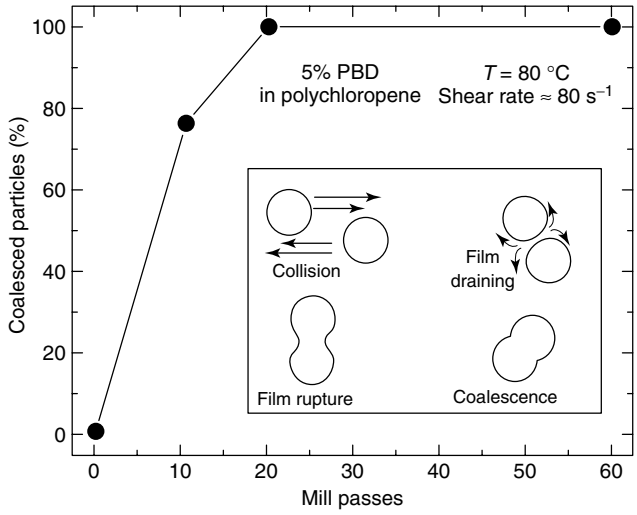

Figure 28 Amount of polybutadiene dispersed in polychloroprene that has coalesced with other dispersed particles versus the extent of mixing (i.e. number of passes through a two-roll mill) at the indicated conditions. The mean particle radius was 40 nm. Coalescence was reflected in the reduction in scattering intensity. The inset shows an idealized depiction of shear-induced coalescence of dispersed particles (from the study by Roland and Bohm[79]).

geometry (sample sheared in the gap between two cylinders).[81]

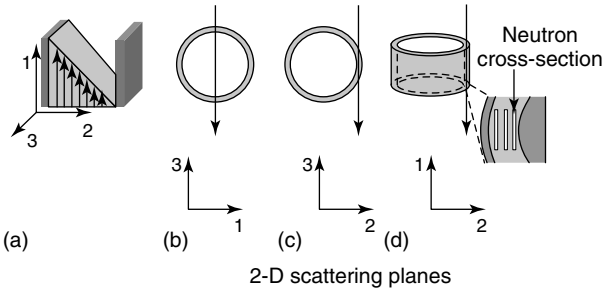

Figure 29 Couette flow geometries showing the different scattering planes. 1 is the flow direction, 2 the direction of the velocity gradient, and 3 the vorticity direction (Eberle and Porcar[81] with permission).

Flow-induced anisotropy in a poloxamer (poly(ethylene glycol)–poly(propylene glycol)–poly(ethylene glycol) triblock copolymer, an amphiphilic material) sheared in a cone and plate device is seen in the transition of Debye–Scherer rings in the scattering pattern from the quiescent material to sharp reflections (Figure 30).[82] Figure 31 compares for a similar material in deuterated water the scattering in the radial direction (the usual measurement geometry) with SANS in the tangential direction.[83] The tangential scattering provides information about the stacking of the 2-D layers.

SANS of concentrated aqueous solutions of poloxamers exhibit peaks corresponding to cubically packed spherical micelles (Figure 32).[84] The domain morphology and hence scattering patterns show hysteresis during traversal of the order–disorder transition.

Rheo-SANS was used to determine the radius of gyration of entangled polystyrene in the nonlinear flow regime (Figure 33).[85] The sample was subjected to recirculating flow through a slit, with the scattering measured both parallel and perpendicular to the flow.

SANS is an attractive technique for characterizing the complex, hierarchical structure of biopolymers, particularly in their natural environment. The number of such studies, including rheo-SANS experiments, has proliferated in recent years.[86–92] Plotted in Figure 34 are various properties of fibrin, a highly branched, cross-linked mesh integral to blood clotting, determined using rheo-SANS.[93]

4.4 Neutron Reflection

Less common than neutron scattering, neutron reflection (NR) is used to probe the structure normal to an interface.[94–97] The neutron reflectivity, $R(Q)$, defined as the ratio of the reflected and incident elastic scattering intensities, is given to a good approximation by[94]:

$$R(Q) = \frac{16\pi^2}{Q^4}\left|F\left(\frac{\mathrm{d}\hat{\rho}}{\mathrm{d}z}\right)\right|^2 \qquad (17)$$

Encyclopedia of Analytical Chemistry, Online © 2006–2012 John Wiley & Sons, Ltd.
This article is © 2012 John Wiley & Sons, Ltd.
This article was published in the *Encyclopedia of Analytical Chemistry* in 2012 by John Wiley & Sons, Ltd.
DOI: 10.1002/9780470027318.a2022.pub2

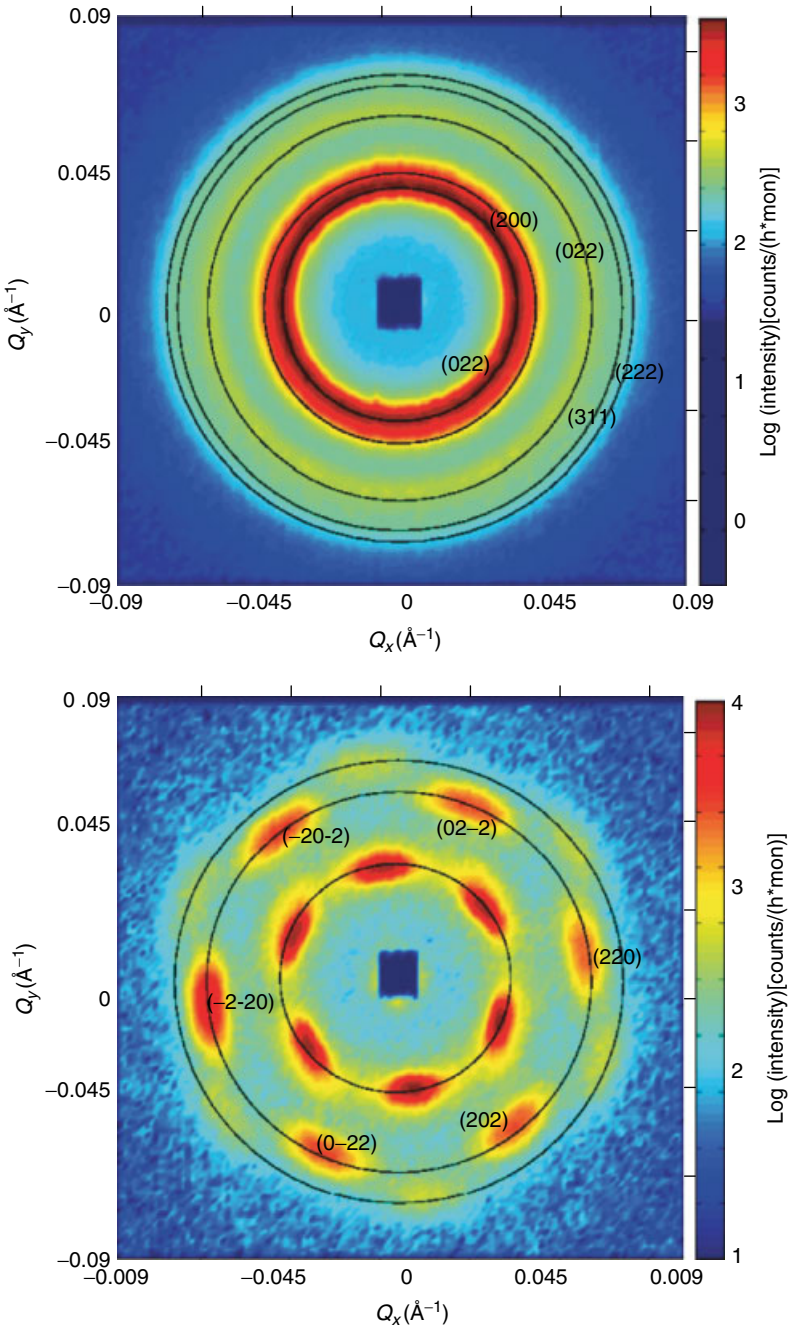

Figure 30 SANS from a poloxamer in transmission mode: (top) no flow (bottom) shearing at 100 s^{-1}. The annotations identify the Debye–Scherer reflections from the face-centered-cubic morphology (from the study by Wolff and Zabel[82] with permission).

where F represents the Fourier transform of the scattering length density profile and z is the dimension perpendicular to the surface. In practice, analyses of NR experiments rely on fitting models to the data, which means the solutions are not always unique. $R(Q)$ is measured as a function of Q, typically over a range of ca. 0.01–0.2 Å^{-1}, obtained by changing either the neutron wavelength or the grazing angle. The Q^{-4} dependence (Fresnel's law) in Equation (17) assumes a perfectly smooth interface; surface roughness causes $R(Q)$ to decrease more strongly with angle. This can limit the attainable Q, but in favorable cases provides information about the surface topography.[98]

The reflectivity yields information on layer composition, thicknesses, and roughness as a function of depth perpendicular to the surface. NR is specular (neutrons

Encyclopedia of Analytical Chemistry, Online © 2006–2012 John Wiley & Sons, Ltd.
This article is © 2012 John Wiley & Sons, Ltd.
This article was published in the *Encyclopedia of Analytical Chemistry* in 2012 by John Wiley & Sons, Ltd.
DOI: 10.1002/9780470027318.a2022.pub2

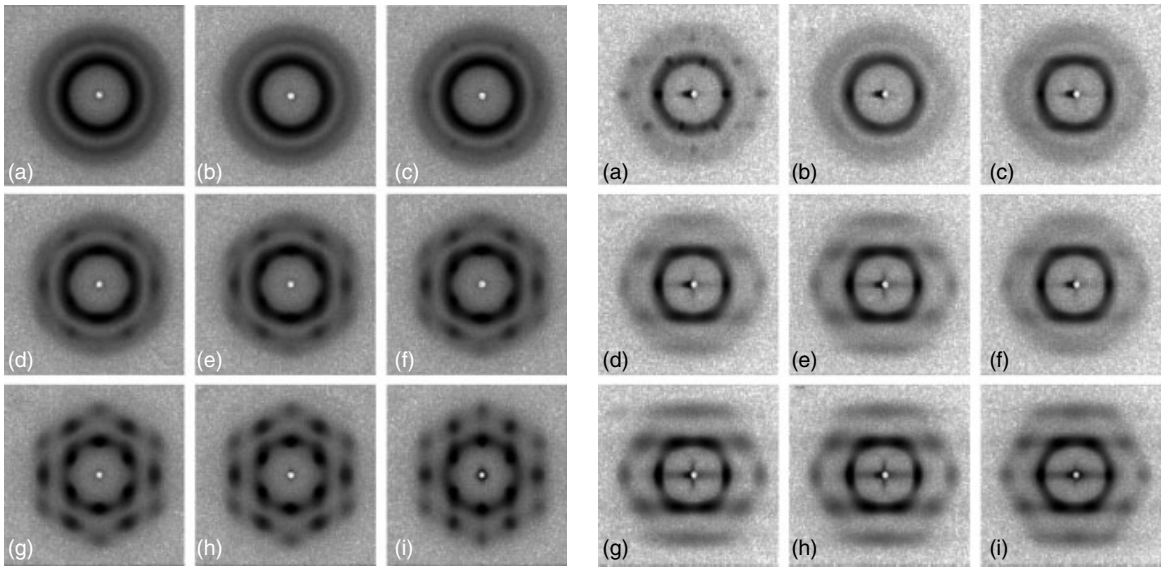

Figure 31 SANS radial (left) and tangential (right) patterns for a poloxamer solution sheared in a Couette apparatus at shear rates (a through i) equal to 0, 0.01, 1, 5, 10, 15, 30, 50, and 600 s^{-1} (from the study by Jiang et al.[83] with permission).

from a single incoming direction are reflected in a single outgoing direction), and the reflected intensity depends only on the scattering length densities; thus, the method cannot distinguish material variations from physical roughness. Diffuse (off-specular) NR can be used to characterize the in-plane composition and lateral variations of structure.[99]

NR finds application in biological materials, where the ability to contrast match is very important, given the complexity of the structures.[100] For example, the

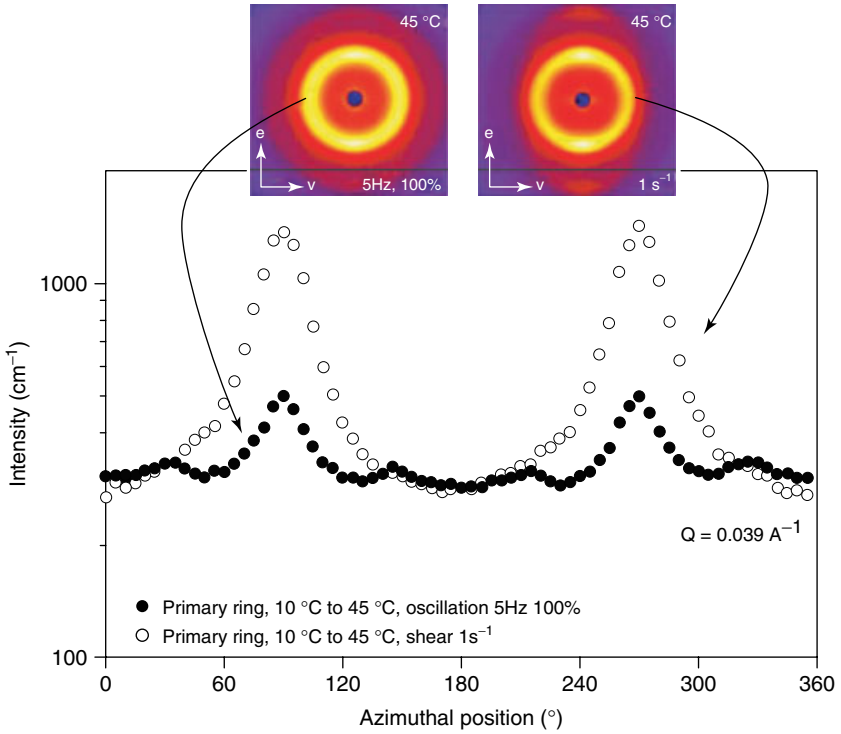

Figure 32 Rheo-SANS profiles and azimuthal intensities measured radially for a poloxamer solution under oscillation (2-D pattern on left and filled symbols) and during steady flow (2-D pattern on right and open symbols). The hexagonally packed cylinder phase is present during oscillation but is disrupted by steady shearing (LaFollette and Walker[84] with permission).

Encyclopedia of Analytical Chemistry, Online © 2006–2012 John Wiley & Sons, Ltd.
This article is © 2012 John Wiley & Sons, Ltd.
This article was published in the *Encyclopedia of Analytical Chemistry* in 2012 by John Wiley & Sons, Ltd.
DOI: 10.1002/9780470027318.a2022.pub2

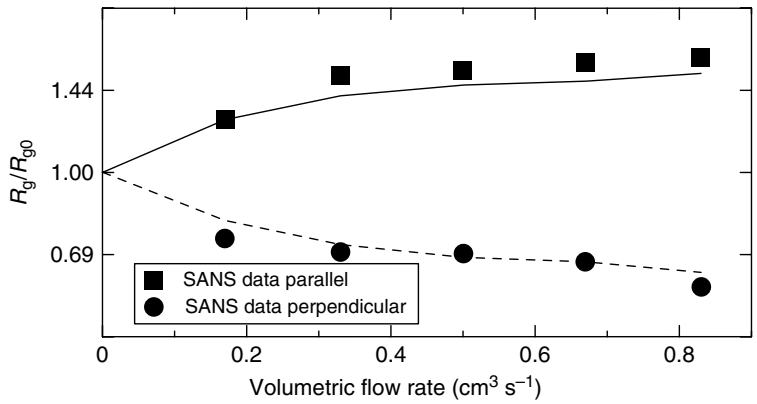

Figure 33 Radius of gyration of polystyrene as a function of flow rate, determined from fitting the Debye function (Equation 8) to the SANS data. The anisotropy begins to level off at higher flow rates (Graham et al.[85] with permission).

ratio of protons and deuterons can be adjusted to eliminate the contribution of water. This is illustrated in Figure 35[101]; the contrast was varied to characterize the layers, with the amount of heavy water changed to selectively emphasizing different components of the membrane.

NR has been applied to the study of the interfacial configuration of macromolecules with unusual architectures, such as brush polymers.[102–104] Figure 36[104] shows a Porod plots (Equation 13) of NR data for a polymer brush grafted onto a gold substrate and immersed in heavy water. From the measured reflectivity, the polymer concentration profile was determined as

$$\varphi(z) = \frac{\hat{\rho}(z) - \hat{\rho}_{sub}}{\hat{\rho}_{poly} - \hat{\rho}_{sub}} \tag{18}$$

where $\hat{\rho}_{poly}$ and $\hat{\rho}_{sub}$ are the respective scattering length densities of the polymer brush and the substrate and z is the distance from the surface. The total amount of polymer at the interface was constant, but its spatial distribution varied in accord with its compatibility with water. The obtained depth profiles are shown in Figure 37.[104] As the temperature is increased above the LCST, there is partial phase separation normal to the surface, resulting in a denser inner phase and a dilute outer phase.

A similar approach can be used to measure the interdiffusion at the interface of two polymers.[105–107] Model calculations are carried out that yield $\hat{\rho}_{poly}$ that fit the experimental reflectivities. Results for interdiffusion of polystyrene with its deuterated analog are shown in Figure 38.[107]

Figure 39 shows the interfacial profile for a bilayer of 1,4-polybutadiene with various rubbers.[105] The peel adhesion measured for the different adherends increases in proportion to the extent of interpenetration, the latter measured by NR.

Other applications of NR include investigating block copolymer morphologies,[108–110] the mobility of polymer segments in confined geometries,[111,112] and examining the interface and adhesion of polymers on substrates.[113,114] Instruments to carry out in situ NR on samples undergoing shear flow have been developed.[115]

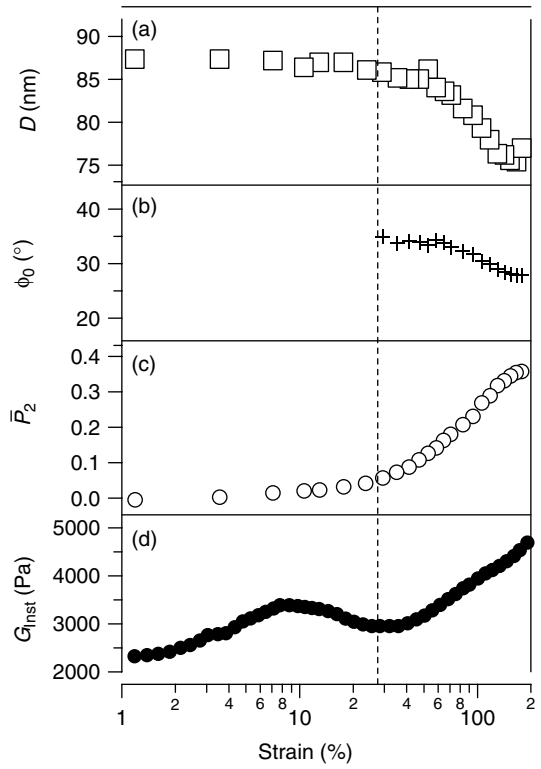

Figure 34 Diameter (a), alignment angle (b), order parameter (c), and instantaneous modulus (d) of fibrin fibers as a function of shear strain (from the study by Weigandt et al.[93] with permission).

Encyclopedia of Analytical Chemistry, Online © 2006–2012 John Wiley & Sons, Ltd.
This article is © 2012 John Wiley & Sons, Ltd.
This article was published in the *Encyclopedia of Analytical Chemistry* in 2012 by John Wiley & Sons, Ltd.
DOI: 10.1002/9780470027318.a2022.pub2

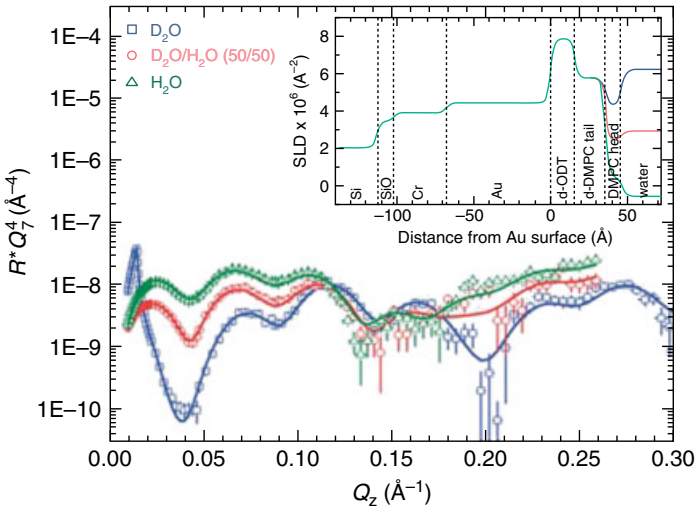

Figure 35 Neutron reflectivity versus momentum transfer for hybrid bilayer membranes with three contrast levels: D_2O (lower curve), 50/50 D_2O/H_2O (middle curve), and H_2O (upper curve). The inset is the scattering length density obtained from modeling the reflectivity data (from the study by Smith et al.[101] with permission).

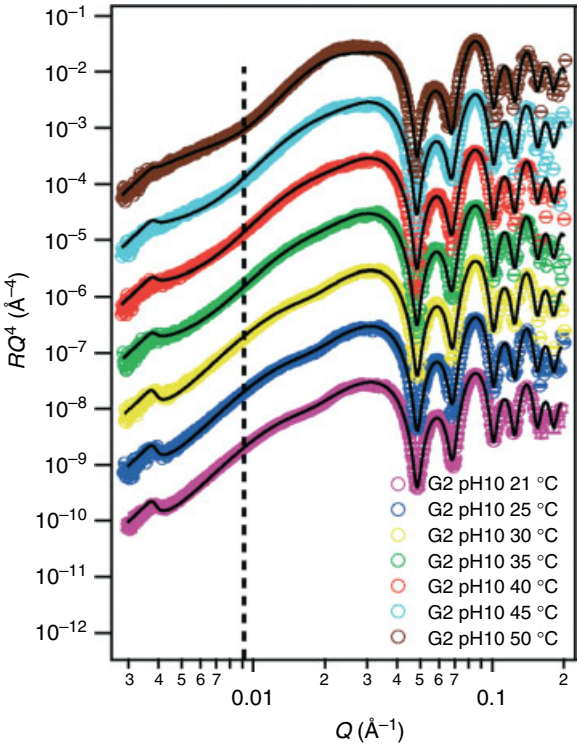

Figure 36 Porod plots of neutron reflectivity measured from polymer brush grafted to a gold substrate as a function of temperature. Solid lines are fits to the NR data. Curves are vertically displaced for clarity (from the study by Jia et al.[104] with permission).

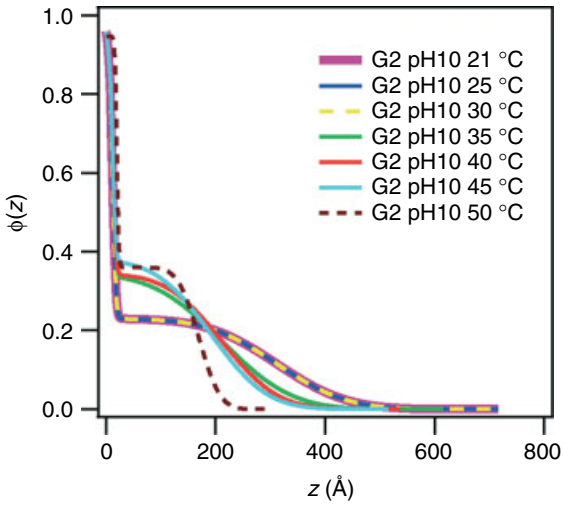

Figure 37 Interfacial polymer profiles determined from the data in Figure 36 for various temperatures. The LCST is between 30 and 40 °C (from the study by Jia et al.[104] with permission).

4.5 Polymer Dynamics

Figure 40 compares the coherent dynamic structure factor for polyethylene oxide rings, linear chains, and their mixture at $Q = 0.05$ Å^{-1}.[116] The faster decay for rings is consistent with their lower melt viscosity.

As stated, an important advantage of neutron scattering over more conventional relaxation spectroscopies is the ability to measure the dynamics at different length scales. Figure 41 shows the change in the breadth of the incoherent QENS spectra with scattering vector for polyethylene.[117] Small Q measurements probe the dynamics within the 'cage' (first coordination shell) of neighboring atoms, while the higher Q data are sensitive to the chain dynamics.

The motion of polyethylene oxide chains adsorbed on clay was monitored using NSE.[118] The data (Figure 42)

Encyclopedia of Analytical Chemistry, Online © 2006–2012 John Wiley & Sons, Ltd.
This article is © 2012 John Wiley & Sons, Ltd.
This article was published in the *Encyclopedia of Analytical Chemistry* in 2012 by John Wiley & Sons, Ltd.
DOI: 10.1002/9780470027318.a2022.pub2

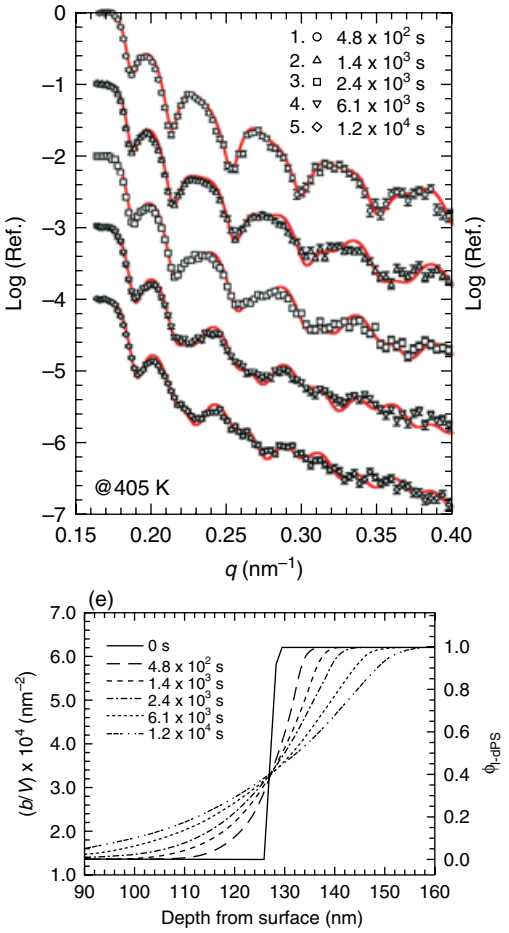

Figure 38 (top) NR profiles for various contact times, vertically offset for clarity; (bottom) model scattering length profiles for a polystyrene/D-polystyrene bilayer film (from the study by Kawaguchi et al.[107] with permission).

conform to Zimm scaling, according to which the relaxation time varies as[119]

$$\tau \propto Q^{-3}\eta/T \qquad (19)$$

where η is the viscosity. The data measured at different scattering vectors collapse to a single master curve when plotted versus the produce of time and Q^3.

5 SUMMARY

Neutron scattering is a powerful analytical tool for investigating polymers. Unique aspects such as the capacity to measure thick samples with an absence heating or radiation-induced damage, selective control of the scattering contrast by isotopic substitution, and the measurement of dynamic properties as a function of length scale are among the many attributes that

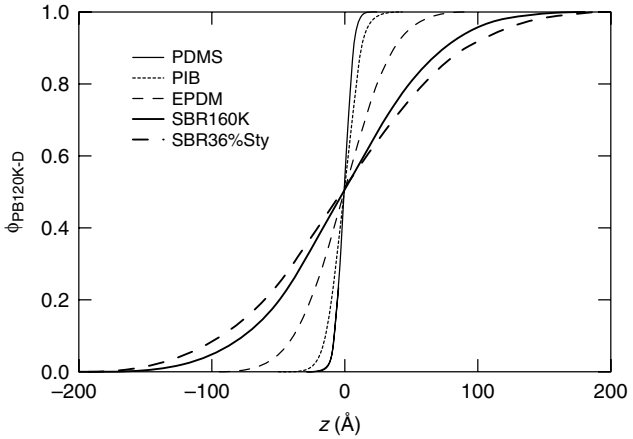

Figure 39 Volume fraction of deuterated polybutadiene at the interface with various polymers, as determined by neutron reflectivity. The strongly incompatible polydimethylsiloxane and polyisobutylene adherends form sharp interfaces (15- to 30-Å breadth), whereas the styrene–butadiene copolymer of lower styrene content gives a broad interface (~200 Å) with the polybutadiene (from the study by Schach et al.[105] with permission).

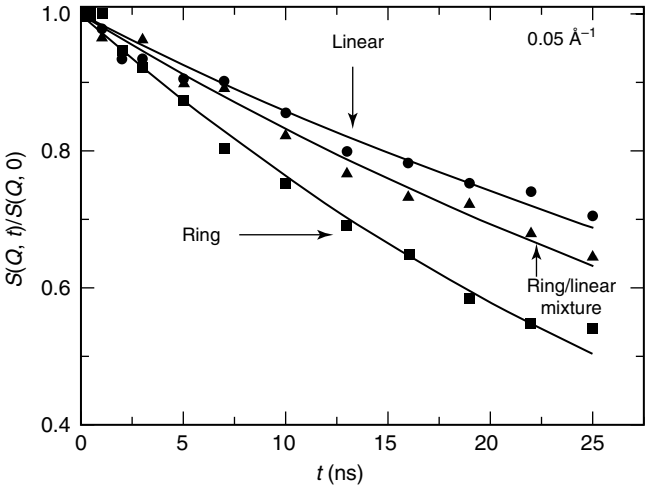

Figure 40 NSE scattering curves for different topologies of polyethylene oxide, showing the faster dynamics of rings compared with linear chains having the same molecular weight. The solid lines are fits to the Rouse model (from Bras et al.[116] with permission).

make neutron methods not just complementary to other analytical techniques, but in many cases the only means to address material issues. The information that can be obtained from neutron scattering – the size, form, and orientation of molecular chains, the thermodynamics and phase structure of mixtures, interfaces and interfacial phenomena, the dynamics at both the local and global length scales, details of the structure of complex nanocomposites and biological materials, etc. – has only been surveyed herein. It is a testament to the

Encyclopedia of Analytical Chemistry, Online © 2006–2012 John Wiley & Sons, Ltd.
This article is © 2012 John Wiley & Sons, Ltd.
This article was published in the *Encyclopedia of Analytical Chemistry* in 2012 by John Wiley & Sons, Ltd.
DOI: 10.1002/9780470027318.a2022.pub2

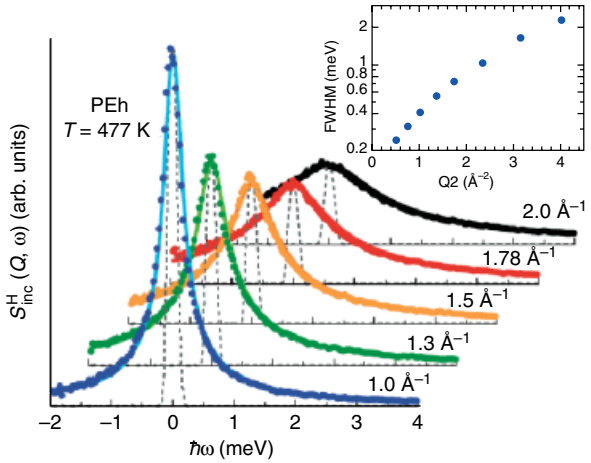

Figure 41 Time-of-flight neutron scattering spectra for polyethylene at various Q and $T = 477$ K. The dotted lines indicate the instrumental resolution. The peak breadth is plotted in the inset versus Q^2; a broader peak signifies faster motion (from the study by Arbe and Colmenero[117] with permission).

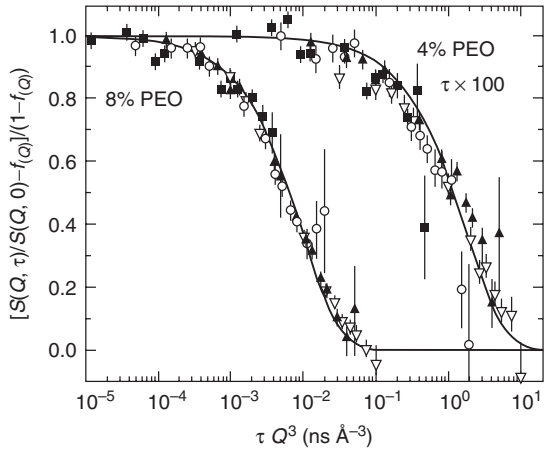

Figure 42 Intermediate scattering function versus the product of time and the cube of the scattering vector for two concentrations of PEO/clay solutions in heavy water. The superposition of the curves for different Q is consistent with Zimm scaling (Equation 19) (from the study by Frielinghaus et al.[118] with permission).

utility of neutron scattering that even though the application of neutrons to polymers did not begin in earnest until the 1990s, through the past decade, about 325 peer-reviewed publications per year have appeared on the topic. Whether this figure changes in the future will likely depend on the availability of the specialized, costly facilities required for neutron experiments. Certainly there is no expectation of abatement in the number of important problems in polymer science that can be addressed using neutron methods.

ACKNOWLEDGMENTS

This work was supported by the Office of Naval Research.

ABBREVIATIONS AND ACRONYMS

2-D	two-dimensional
LCST	lower critical solution temperature
NMR	nuclear magnetic resonance
NR	neutron reflection
NSE	neutron spin echo
PEO	polyethylene oxide
PMMA	polymethymethacrylate
POSS	Polyhedral oligomeric silsesquioxane
QENS	quasielastic neutron scattering
RPA	random phase approximation
SANS	Small-angle neutron scattering
SAXS	Small-angle X-ray scattering
USANS	ultra-small-angle neutron scattering
WANS	wide-angle neutron scattering

RELATED ARTICLES

Particle Size Analysis **(Volume 6)**
Light Scattering, Classical: Size and Size Distribution Characterization

Polymers and Rubbers **(Volume 8)**
Polymers and Rubbers: Introduction

Polymers and Rubbers **(Volume 9)**
Infrared Spectroscopy in Analysis of Polymer Structure–Property Relationships • Infrared Spectroscopy in Analysis of Polymers and Rubbers • Near-infrared Spectroscopy of Polymers and Rubbers • Nuclear Magnetic Resonance, Solid state in Analysis of Polymers and Rubbers • X-ray Scattering in Analysis of Polymers

Surfaces **(Volume 10)**
Ellipsometry in Analysis of Surfaces and Thin Films

Nuclear Methods **(Volume 14)**
Rutherford Backscattering Spectroscopy

REFERENCES

1. U. Bonse, M. Hart, 'Tailless X-Ray Single-Crystal Reflection Curves Obtained By Multiple Reflection', *Appl. Phys. Lett.*, **7**, 238–240 1965.
2. M. Villa, M. Baron, M. Hainbuchner, E. Jericha, V. Leiner, D. Schwahn, E. Seidl, J. Stahn, H. Rauch, 'Optimisation of a Crystal Design for a Bonse-Hart Camera', *J. Appl. Crystallogr.*, **36**, 769–773 2003.

Encyclopedia of Analytical Chemistry, Online © 2006–2012 John Wiley & Sons, Ltd.
This article is © 2012 John Wiley & Sons, Ltd.
This article was published in the *Encyclopedia of Analytical Chemistry* in 2012 by John Wiley & Sons, Ltd.
DOI: 10.1002/9780470027318.a2022.pub2

3. S. Borbely, M. Heiderich, D. Schwahn, E. Seidl, 'Resolution of the USANS Diffractometer at the FRJ-2 Research R in Julich', *Physica B*, **276**, 138–139 2000.
4. M. Agamalian, G.D. Wignall, R. Triolo, 'Optimization of a Bonse–Hart Ultra-Small-Angle Neutron Scattering Facility by Elimination of the Rocking-Curve Wings', *J. Appl. Crystallogr.*, **30**, 3435–3352 1997.
5. I. Bako, G. Palinkas, J.C. Doreb, H. Fischer, P. Jovari, 'Wide and Low Angle Neutron Scattering of Water–Pyridine Mixtures', *Chem. Phys. Lett.*, **388**, 468–472 2004.
6. G.D. Wignall, L. Mandelkern, C. Edwards, M. Glotin, 'Wide-Angle Neutron Scattering Studies of Mixed Crystals of Polyethylene and Deuteropolyethylene', *J. Polym. Sci., Polym. Phys. Ed.*, **20**, 245–258 1982.
7. F.S. Bates, G.D. Wignall, W.C. Koehler, 'Critical Behavior of Binary-liquid Mixtures of Deuterated and Protonated Polymers', *Phys. Rev. Lett.*, **55**, 2425–2428 1985.
8. A. Lapp, C. Picot, H. Benoit, 'Determination of the Flory Interaction Parameters in Miscible Polymer Blends by Measurement of the Apparent Radius of Gyration', *Macromolecules*, **18**, 2437–2441 1985.
9. C.M. Roland, C.A. Trask, 'Miscibility Limits in Poly(vinylethylene) Isotopic Mixtures', *Polym. Bull.*, **20**, 471–478 1988.
10. J.D. Londono, A.H. Narten, G.D. Wignall, K.G. Honnell, E.T. Hsieh, T.W. Johnson, F.S. Bates, 'Composition Dependence of the Interaction Parameter in Isotopic Polymer Blends', *Macromolecules*, **27**, 2864–2871 1994.
11. P.G. de Gennes, *Scaling Concepts in Polymer Physics*, Cornell University Press, New York, 1979.
12. A. Papon, H. Montes, F. Lequeux, J. Oberdisse, K. Saalwachter, L. Guy, 'Solid Particles in an Elastomer Matrix: Impact of Colloid Dispersion and Polymer Mobility Modification on the Mechanical Properties', *Soft Matter*, **8**, 4090–4096 2012.
13. R.J. Roe, *Methods of X-Ray and Neutron Scattering in Polymer Science*, Oxford Univ. Press, New York, 2000.
14. R. Hempelmann, *Quasielastic Neutron Scattering and Solid State Diffusion*, Clarendon Press, Oxford, 2000.
15. C.M. Roland, *Viscoelastic Behavior of Rubbery Materials*, Oxford Univ. Press, Oxford, 2011.
16. A. Guinier, 'Diffraction of X-rays at Small Angles: Application to the Study of Microscopic Phenomena', *Ann. Phys. (Paris)*, **12**, 161–237 1939.
17. A. Guinier, 'The Diffusion of X-Rays under the Extremely Weak Angles Applied to the Study of Fine Particles and Colloidal Suspension', *Comptes Rendus*, **206**, 1374–1376 1938.
18. B.H. Zimm, 'Dynamics of Polymer Molecules in Dilute Solution - Viscoelasticity, Flow Birefringence, and Dielectric Loss', *J. Chem. Phys.*, **24**, 269–278 1956.
19. J. Stellbrink, L. Willner, O. Jucknischke, D. Richter, P. Lindner, L.J. Fetters, J.S. Huang, 'Self-Assembling Behavior of Living Polymers', *Macromolecules*, **31**, 4189–4197 1998.
20. K. Mayumi, N. Osaka, H. Endo, H. Yokoyama, Y. Sakai, M. Shibayama, K. Ito, 'Concentration-Induced Conformational Change in Linear Polymer Threaded into Cyclic Molecules', *Macromolecules*, **41**, 6480–6485 2008.
21. P. Debye, 'Molecular Weight Determination by Light Scattering', *J. Phys. Coll. Chem.*, **51**, 18–32 1947.
22. O. Kratky, G. Porod, 'X-Ray Study of Dissolved Molecular Threads', *J. R. Neth. Chem. Soc.*, **68**, 1106–1122 1949.
23. S.I. Yun, K.-C. Lai, R.M. Briber, S.J. Teertstra, M. Gauthier, B.J. Bauer, 'Conformation of Arborescent Polymers in Solution by Small-Angle Neutron Scattering: Segment Density and Core-Shell Morphology', *Macromolecules*, **41**, 175–183 2008.
24. B. Hammouda, 'SANS from Homogeneous Polymer Mixtures: A Unified Overview', *Adv. Polym. Sci.*, **106**, 87–133 1993.
25. C.C. Han, B.J. Bauer, J.C. Clark, Y. Muroga, Y. Matsushita, M. Okada, T.C. Qui, T.H. Chang, I.C. Sanchez, 'Temperature, Composition and Molecular-weight Dependence of the Binary Interaction Parameter of Polystyrene–Poly(Vinyl Methyl Ether) Blends', *Polymer*, **29**, 2002–2014 1988.
26. J.D. Londono, G.D. Wignall, 'The Flory–Huggins Interaction Parameter in Blends of Polystyrene and Poly(p-methylstyrene) by Small-angle Neutron Scattering', *Macromolecules*, **30**, 3821–3824 1997.
27. D.W. Tomlin, C.M. Roland, 'Negative Excess Enthalpy in a van der Waals Polymer Mixture', *Macromolecules*, **25**, 2994–2996 1992.
28. P. Debye, A.M. Bueche, 'Scattering by An Inhomogeneous Solid', *J. Appl. Phys.*, **20**, 518–525 1949.
29. A.R. Hopkins, S.J. Tomczak, V. Vij, A.J. Jackson, 'Small Angle Neutron Scattering (SANS) Characterization of Electrically Conducting Polyaniline Nanofiber/Polyimide Nanocomposites', *Thin Solid Films*, **520**, 1617–1620 2011.
30. K.M. Dean, W.D. Cook, M.Y. Lin, 'Small Angle Neutron Scattering and Dynamic Mechanical Thermal Analysis of Dimethacrylate/Epoxy IPNs', *Eur. Polym. J.*, **42**, 2872–2887 2006.
31. N.P. Balsara, T.J. Rappl, A.A. Lefebvre, 'Does Conventional Nucleation Occur During Phase Separation in Polymer Blends?' *J. Polym. Sci., Polym. Phys. Ed.*, **42**, 1793–1809 2004.
32. N.S. Wanakule, A.J. Nedoma, M.L. Robertson, Z. Fang, A. Jackson, B.A. Garetz, N.P. Balsara, 'Characterization

Encyclopedia of Analytical Chemistry, Online © 2006–2012 John Wiley & Sons, Ltd.
This article is © 2012 John Wiley & Sons, Ltd.
This article was published in the *Encyclopedia of Analytical Chemistry* in 2012 by John Wiley & Sons, Ltd.
DOI: 10.1002/9780470027318.a2022.pub2

of Micron-Sized Periodic Structures in Multicomponent Polymer Blends by Ultra-Small-Angle Neutron Scattering and Optical Microscopy', *Macromolecules*, **41**, 471–477 2008.

33. K. Krishnan, B. Chapman, F.S. Bates, T.P. Lodge, K. Almdal, W.R. Burghardt, 'Effects of Shear Flow on a Polymeric Bicontinuous Microemulsion: Equilibrium and Steady State Behavior', *J. Rheol.*, **46**, 529–554 2002.
34. A.A. Lefebvre, J.H. Lee, N.P. Balsara, C. Vaidyanathan, 'Determination of Critical Length Scales and the Limit of Metastability In Phase Separating Polymer Blends', *J. Chem. Phys.*, **117**, 9063–9073 2002.
35. T.J. Shin, B. Lee, B.S. Seong, Y.S. Han, C.-H. Lee, H.H. Song, R.S. Stein, M. Ree, 'Composition-Dependent Phase Segregation and Cocrystallization Behaviors of Blends of Metallocene-Catalyzed Octene-LLDPE(D) and LDPE(H)', *Polymer*, **51**, 5799–5806 2010.
36. G. Porod, 'The Small Angle X-Ray Scattering of Tightly Packed Colloids Systems. Part I', *Colloid Polym. Sci.*, **124**, 83–114 1951.
37. M.A. Sharp, P.K. Pranzas, A. Schreyer, 'Going Ultra: How We Can Increase the Length Scales Studied in Small-Angle Neutron Scattering', *Adv. Eng. Mater.*, **11**, 441–445 2009.
38. T. Kanaya, H. Takeshita, Y. Nishikoji, M. Ohkura, K. Nishida, K. Kaji, 'Micro- and Mesoscopic Structure of Poly(vinyl alcohol) Gels Determined by Neutron and Light Scattering', *Supramol. Sci.*, **5**, 215–221 1998.
39. L. van Hove, 'Correlations in Space and Time and Born Approximation Scattering in Systems of Interacting Particles', *Phys. Rev.*, **95**, 249–262 1954.
40. K. Sinha, J.K. Maranas, 'Segmental Dynamics and Ion Association in PEO-Based Single Ion Conductors', *Macromolecules*, **44**, 5381–5391 2011.
41. A. Arbe, A.-C. Genix, S. Arrese-Igor, J. Colmenero, D. Richter, 'Dynamics in Poly(n-alkyl methacrylates): A Neutron Scattering, Calorimetric, and Dielectric Study', *Macromolecules*, **43**, 3107–3119 2010.
42. U. Keiderling, A. Wiedenmann, J. Haug, 'Stroboscopic Time-Resolved SANS Technique for Dynamical Studies of Slow Relaxation Processes', *Physica B*, **385–386**, 1183–1186 2006.
43. B. Frick, C. Alba-Simionesco, K.H. Andersen, L. Willner, 'Influence of Density and Temperature on the Microscopic Structure and the Segmental Relaxation of Polybutadiene', *Phys. Rev.*, **E67**, 051801 2003.
44. A.Z. Akcasu, G.C. Summerfield, S.N. Jahshan, C.C. Han, C.Y. Kim, and H. Yu, 'Measurement of Single Chain Neutron Scattering in Concentrated Polymer Solutions', *J. Polym. Sci., Polym. Phys. Ed.*, **18**, 863–869 1980.
45. R. Ramachandran, G. Beaucage, D. McFaddin, J. Merrick-Mack, V. Galiatsatos, F. Mirabella, 'Branch Length Distribution in TREF Fractionated Polyethylene', *Polymer*, **52**, 2661–2666 2011.
46. R. Ramachandran, G. Beaucage, A.S. Kulkarni, D. McFaddin, J. Merrick-Mack, V. Galiatsatos, 'Persistence Length of Short-Chain Branched Polyethylene', *Macromolecules*, **41**, 9802–9806 2008.
47. T. Terashima, R. Motokawa, S. Koizumi, M. Sawamoto, M. Kamigaito, T. Ando, T. Hashimoto, 'In Situ and Time-Resolved Small-Angle Neutron Scattering Observation of Star Polymer Formation via Arm-Linking Reaction in Ruthenium-Catalyzed Living Radical Polymerization', *Macromolecules*, **43**, 8218–8232 2010.
48. S. Koizumi, 'Gel-Like Aspect of a Miscible Polymer Mixture Studied by Small-Angle Neutron Scattering', *J. Polym. Sci., Polym. Phys. Ed.*, **42**, 3148–3164 2004.
49. J.T. Cabral, J.S. Higgins, 'Small Angle Neutron Scattering from the Highly Interacting Polymer Mixture TMPC/Psd: No Evidence of Spatially Dependent Chi Parameter', *Macromolecules*, **42**, 9528–9536 2009.
50. D. Schwahn, V. Pipich, D. Richter, 'Composition and Long-Range Density Fluctuations in PEO/PMMA Polymer Blends: A Result of Asymmetric Component Mobility', *Macromolecules*, **45**, 2035–2049 2012.
51. A.J. Nedoma, P. Lai, A. Jackson, M.L. Robertson, N.P. Balsara, 'Phase Behavior of Off-Critical A/B/A-C Blends', *Macromolecules*, **43**, 7852–7859 2010.
52. F.S. Bates, G.H. Fredrickson, 'Block Copolymers – Designer Soft Materials', *Physics Today*, **52**, 32–38 1999.
53. J. Rodriguez-Hernandez, F. Checot, Y. Gnanou, S. Lecommandoux, 'Toward 'Smart' Nano-Objects by Self-Assembly of Block Copolymers in Solution', *Prog. Polym. Sci.*, **30**, 691–724 2005.
54. S.B. Darling, 'Directing the Self-Assembly of Block Copolymers', *Prog. Polym. Sci.*, **32**, 1152–1120 2007.
55. F.S. Bates, M.A. Hillmyer, T.P. Lodge, C.M. Bates, K.T. Delaney, G.H. Fredrickson, 'Multiblock Polymers: Panacea or Pandora's Box?' *Science*, **336**, 434–440 2012.
56. R.W. Richards, 'Small-Angle Neutron Scattering Studies of Polymers: Selected Aspects', *J. Macromol. Sci., Chem*, **A26**, 787–815 1989.
57. T.A. Shefelbine, M.E. Vigild, M.W. Matsen, D.A. Hajduk, M.A. Hillmyer, E.L. Cussler, F.S. Bates, 'Core-Shell Gyroid Morphology in a Poly(isoprene-block-styrene-block-dimethylsiloxane) Triblock Copolymer', *J. Am. Chem. Soc.*, **121**, 8457–8465 1999.
58. M.W. Matsen, F.S. Bates, 'Unifying Weak- and Strong-Segregation Block Copolymer Theories', *Macromolecules*, **29**, 1091–1098 1996.
59. I. Krakovsky, N.K. Szekely, 'SANS and DSC Study of Water Distribution in Epoxy-Based Hydrogels', *Eur. Polym. J.*, **47**, 2177–2188 2011.

Encyclopedia of Analytical Chemistry, Online © 2006–2012 John Wiley & Sons, Ltd.
This article is © 2012 John Wiley & Sons, Ltd.
This article was published in the *Encyclopedia of Analytical Chemistry* in 2012 by John Wiley & Sons, Ltd.
DOI: 10.1002/9780470027318.a2022.pub2

60. J.S. Pedersen, 'Determination of Size Distribution from Small-Angle Scattering Data for Systems with Effective Hard-Sphere Interactions', *J. Appl. Cryst.*, **27**, 595–608 1994.

61. Z. Sun, C.D. Tomlin, E.M. Sevick-Muraca, 'Approach for Particle Sizing in Dense Polydisperse Colloidal Suspension Using Multiple Scattered Light', *Langmuir*, **17**, 6142–6147 2001.

62. R. Inoubli, S. Dagreou, A. Lapp, L. Billon, J. Peyrelasse, 'Nanostructure and Mechanical Properties of Polybutylacrylate Filled with Grafted Silica Particles', *Langmuir*, **22**, 6683–6689 2006.

63. T. Koga, T. Hashimoto, M. Takenaka, K. Aizawa, N. Amino, M. Nakamura, D. Yamaguchi, S.K. Hashimoto., 'New Insight into Hierarchical Structures of Carbon Black Dispersed in Polymer Matrices: A Combined Small-Angle Scattering Study', *Macromolecules*, **41**, 453–464 2008.

64. F. Nettesheim, M.W. Liberatore, T.K. Hodgdon, N.J. Wagner, E.W. Kaler, M. Vethamuthu, 'Influence of Nanoparticle Addition on the Properties of Wormlike Micellar Solutions', *Langmuir*, **24**, 7718–7726 2008.

65. D.C. Pozzo, L.M. Walker, 'Macroscopic Alignment of Nanoparticle Arrays in Soft Crystals of Cubic and Cylindrical Polymer Micelles', *Eur. Phys. J. E*, **26**, 183–189 2008.

66. M. Takeda, T. Matsunaga, T. Nishida, H. Endo, T. Takahashi, M. Shibayama, 'Rheo-SANS Studies on Shear Thickening in Clay-Poly(ethylene oxide) Mixed Solutions', *Macromolecues*, **43**, 7793–7799 2010.

67. B. Chu, T. Liu, 'Characterization of Nanoparticles by Scattering Techniques', *J. Nanoparticle Res.*, **2**, 29–41 2000.

68. N. Jouault, P. Vallat, F. Dalmas, S. Said, J. Jestin, F. Boue, 'Well-Dispersed Fractal Aggregates as Filler in Polymer-Silica Nanocomposites: Long-Range Effects in Rheology', *Macromolecules*, **42**, 2031–2040 2009.

69. K. Nusser, G.J. Schneider, W. Pyckhout-Hintzen, D. Richter, 'Viscosity Decrease and Reinforcement in Polymer-Silsesquioxane Composites', *Macromolecules*, **44**, 7820–7830 2011.

70. W. Zaja, A. Boczkowska, K. Babski, K.J. Kurzydlowski, P.P. Deen, 'Measurements of Residual Strains in Ceramic–Elastomer Composites with Diffuse Scattering of Polarized Neutrons', *Acta Mater.*, **56**, 5964–5971 2008.

71. A. Ramzi, F. Zielinski, J. Bastide, F. Boue, 'Butterfly Patterns: Small-Angle Neutron Scattering from Deuterated Mobile Chains in a Randomly Cross-Linked Polystyrene Network', *Macromolecules*, **28**, 3570–3587 1995.

72. F. Horkay, A.M. Hecht, E. Geissler, 'Fine Structure of Polymer Networks as Revealed by Solvent Swelling', *Macromolecules*, **31**, 8851–8856 1998.

73. S. Koizumi, M. Monkenbusch, D. Richter, D. Schwahn, B. Farago, 'Concentration Fluctuations in Polymer Gel Investigated by Neutron Scattering: Static Inhomogeneity in Swollen Gel', *J. Chem. Phys.*, **121**, 12721–12731 2004.

74. N. de la Rosa-Fox, V. Morales-Florez, J.A. Toledo-Fernandez, M. Pinero, L. Esquivias, U. Keiderling, 'SANS Study of Hybrid Silica Aerogels under ''in situ'' Uniaxial Compression', *J. Sol-Gel Sci. Technol.*, **45**, 245–250 2008.

75. M. Shibayama, 'Small-Angle Neutron Scattering on Polymer Gels: Phase Behavior, Inhomogeneities and Deformation Mechanisms', *Polym. J.*, **43**, 18–34 2011.

76. S. Koizumi, J. Suzuki, 'Three-Dimensional Small-Angle Neutron Scattering of Shear-Induced Phase Separation in a Dynamically Asymmetric Polymer Mixture', *J. Appl. Crystallogr.*, **39**, 878–888 2006.

77. T. Kanaya, G. Matsuba, Y. Ogino, K. Nishida, H.M. Shimizu, T. Shinohara, T. Oku, J. Suzuki, T. Otomo, 'Hierarchic Structure of Shish-Kebab by Neutron Scattering in Wide Q Range', *Macromolecules*, **40**, 3650–3654 2007.

78. S. Koizumi, T. Inoue, 'Dynamical Coupling Between Stress and Concentration Fluctuations in a Dynamically Asymmetric Polymer Mixture, Investigated by Time-Resolved Small-Angle Neutron Scattering Combined with Linear Mechanical Measurements', *Soft Matter*, **7**, 9248–9258 2011.

79. C.M. Roland, G.G.A. Bohm, 'Shear-induced Coalescence in 2-phase Polymeric Systems. 1. Determination From Small-angle Neutron-scattering Measurements', *J. Polym. Sci., Part B: Polym. Phys.*, **22**, 79–93 1984.

80. L. Porcar, D. Pozzo, G. Langenbucher, J. Moyer, P.D. Butler, 'Rheo-Small-Angle Neutron Scattering at the National Institute of Standards and Technology Center for Neutron Research', *Rev. Sci. Instrum.*, **82**, 083902 2011.

81. A.P.R. Eberle, L. Porcar, 'Flow-SANS and Rheo-SANS Aapplied to Soft Matter', *Curr. Opin. Colloid Interface Sci.*, **17**, 33–43 2012.

82. M. Wolff, A. Magerl, H. Zabel, 'NS-SANS for the Investigation of Micellar Systems', *Thin Solid Films*, **515**, 5724–5727 2007.

83. J. Jiang, C. Burger, C. Li, J. Li, M.Y. Lin, R.H. Colby, M.H. Rafailovich, J.C. Sokolov, 'Shear-Induced Layered Structure of Polymeric Micelles by SANS', *Macromolecules*, **40**, 4016–4022 2007.

84. T.A. LaFollette, L.M. Walker, 'Structural and Mechanical Hysteresis at the Order-Order Transition of Block Copolymer Micellar Crystals', *Polymers*, **3**, 281–298 2011.

85. R.S. Graham, J. Bent, N. Clarke, L.R. Hutchings, R.W. Richards, T. Gough, D.M. Hoyle, O.G. Harlen, I. Grillo, D. Auhl, T.C.B. McLeish, 'The Long-Chain

Encyclopedia of Analytical Chemistry, Online © 2006–2012 John Wiley & Sons, Ltd.
This article is © 2012 John Wiley & Sons, Ltd.
This article was published in the *Encyclopedia of Analytical Chemistry* in 2012 by John Wiley & Sons, Ltd.
DOI: 10.1002/9780470027318.a2022.pub2

Dynamics in a Model Homopolymer Blend under Strong Flow: Small-Angle Neutron Scattering and Theory', *Soft Matter*, **5**, 2383–2389 2009.

86. A.K.H. Hirsch, E. Buhler, J.M. Lehn, 'Biodynamers: Self-Organization-Driven Formation of Doubly Dynamic Proteoids', *J. Am. Chem. Soc.*, **134**, 4177–4183 2012.
87. F. Horkay, B. Hammouda, 'Small-Angle Neutron Scattering from Typical Synthetic and Biopolymer Solutions', *Colloid Polym. Sci.*, **286**, 611–620 2008.
88. L.L. Hyland, M.B. Taraban, B. Hammouda Boualem, Y.B. Yu, 'Mutually Reinforced Multicomponent Polysaccharide Networks', *Biopolymers*, **95**, 840–8512011.
89. L.L. Hyland, M.B. Taraban, B. Hammouda Boualem, Y.B. Yu, 'Viscoelastic Properties and Nanoscale Structures of Composite Oligopeptide-Polysaccharide Hydrogels', *Biopolymers*, **97**, 177–188 2011.
90. J.H. Lee, D. Danino, S.R. Raghavan, 'Polymerizable Vesicles Based on a Single-Tailed Fatty Acid Surfactant: A Simple Route to Robust Nanocontainers', *Langmuir*, **25**, 1566–1571 2009.
91. A.N. Gupta, H.B. Bohidar, V.K. Aswal, 'Surface Patch Binding Induced Intermolecular Complexation and Phase Separation in Aqueous Solutions of Similarly Charged Gelatin-Chitosan Molecules', *J. Phys. Chem. B*, **111**, 10137–10145 2007.
92. H. Yan, A. Saiani, J.E. Gough, A.F. Miller, 'Thermoreversible Protein Hydrogel as Cell Scaffold', *Biomacromolecules*, **7**, 2776–2782 2006.
93. K.M. Weigandt, L. Porcar, D.C. Pozzo, 'In situ Neutron Scattering Study of Structural Transitions in Fibrin Networks Under Shear Deformation', *Soft Matter*, **7**, 9992–10000 2011.
94. T.P. Russell, 'X-ray and Neutron Reflectivity for the Investigation of Polymers', *Mater. Sci. Rep.*, **5**, 171–271 1990.
95. J. Penfold, R.M. Richardson, A. Zarbakhsh, J.R.P. Webster, D.G. Bucknall, A.R. Rennie, R.A.L. Jones, T. Cosgrove, R.K. Thomas, J.S. Higgins, P.D.I. Fletcher, E. Dickinson, S.J. Roser, I.A. McLure, A.R. Hillman, R.W. Richards, E.J. Staples, A.N. Burgess, E.A. Simister, J.W. White, 'Recent Advances in the Study of Chemical Surfaces and Interfaces by Specular Neutron Reflection', *J. Chem. Soc., Faraday Trans.*, **93**, 3899–3917 1997.
96. D.G. Bucknall, J.S. Higgins, ''Neutron reflection studies of polymer–polymer interfaces'', in *Polymers and Surfaces – A Versatile Combination*, ed. H. Hommell, Research Signpost, Trivandrum, 161–199, 1998.
97. G. Gragneto-Cusani, 'Neutron Reflectivity at the Solid/Liquid Interface: Examples of Applications in Biophysics', *J. Phys.: Condens. Matter*, **13**, 4973–4989 2001.
98. C.F. Majkrzak, E. Carpenter, F. Heinrich, N.F. Berk, 'When Beauty is Only Skin Deep; Optimizing the Sensitivity of Specular Neutron Reflectivity for Probing Structure Beneath the Surface of Thin Films', *J. Appl. Phys.*, **110**, 102212 2011.
99. K.A. Lavery, V.M. Prabhu, S. Satija, W.L. Wu, 'Lateral Uniformity in Chemical Composition Along a Buried Reaction Front in Polymers Using Off-Specular Reflectivity', *J. Phys.: Condens. Matter*, **22**, 474011 2010.
100. M. Dubey, M.S. Jablin, H. Smith, J. Majewski, 'Investigations of Surrogate Cellular Membranes Using Neutron Reflectometry', *Acta Crystallogr.*, **D66**, 1237–1243 2010.
101. M.B. Smith, D.J. McGillivray, J. Genzer, M. Lösche, P.K. Kilpatrick, 'Neutron Reflectometry of Supported Hybrid Bilayers with Inserted Peptide', *Soft Matter*, **6**, 862–865 2010.
102. N. Schuewer, T. Geue, J.P. Hinestrosa, H.A. Klok, 'Neutron Reflectivity Study on the Postpolymerization Modification of Poly(2-hydroxyethyl methacrylate) Brushes', *Macromolecules*, **44**, 6868–6874 2011.
103. T. Koga, P. Gin, H. Yamaguchi, M.K. Endoh, M. Asada, L. Sendogdular, M. Kobayashi, A. Takahara, B. Akgun, S.K. Satija, T. Sumi, 'Generality of Anomalous Expansion of Polymer Chains in Supercritical Fluids', *Polymer*, **52**, 4331–4336 2011.
104. H. Jia, A. Wildes, S. Titmuss, 'Structure of pH-Responsive Polymer Brushes Grown at the Gold-Water Interface: Dependence on Grafting Density and Temperature', *Macromolecules*, **45**, 305–312 2012.
105. R. Schach, Y. Tran, A. Menelle, C. Creton, 'Role of Chain Interpenetration in the Adhesion between Immiscible Polymer Melts', *Macromolecules*, **40**, 6325–6332 2007.
106. S. Coppee, S. Gabriele, A.M. Jonas, J. Jestin, P. Damman, 'Influence of Chain Interdiffusion Between Immiscible Polymers on Dewetting Dynamics', *Soft Matter*, **7**, 9951–9955 2011.
107. D. Kawaguchi, A. Nelson, Y. Masubuchi, J.P. Majewski, N. Torikai, N.L. Yamada, A.R.S. Sarah, A. Takano, Y. Matsushita, 'Precise Analyses of Short-Time Relaxation at Asymmetric Polystyrene Interface in Terms of Molecular Weight by Time-Resolved Neutron Reflectivity Measurements', *Macromolecules*, **44**, 9424–9433 2011.
108. S.H. Hong, E.J. Lee, K.B. Song, K.H. Lee, 'Homopolymer Distribution in Polystyrene - Poly(methyl methacrylate) Diblock Copolymer', *Polym -Korea*, **35**, 531–536 2011.
109. V. Lauter, P. Mueller-Buschbaum, H. Lauter, W. Petry, 'Morphology of Thin Nanocomposite Films of Asymmetric Diblock Copolymer and Magnetite Nanoparticles', *J. Phys.: Condens. Matter*, **23**, 254215 2011.
110. W. Chen, J.Y. Wang, X.Y. Wei, J. Xu, A.C. Balazs, K. Matyjaszewski, T.P. Russell, 'UV-Enhanced Ordering

Encyclopedia of Analytical Chemistry, Online © 2006–2012 John Wiley & Sons, Ltd.
This article is © 2012 John Wiley & Sons, Ltd.
This article was published in the *Encyclopedia of Analytical Chemistry* in 2012 by John Wiley & Sons, Ltd.
DOI: 10.1002/9780470027318.a2022.pub2

in Azobenzene-Containing Polystyrene-block-Poly(n-Butyl Methacrylate) Copolymer Blends', *Macromolecules*, **44**, 278–285 2011.

111. R. Inoue, K. Kawashima, K. Matsui, M. Nakamura, K. Nishida, T. Kanaya, N.L. Yamada, 'Interfacial Properties of Polystyrene Thin Films as Revealed by Neutron Reflectivity', *Phys. Rev. E*, **84**, 031802 2011.

112. D. Hudzinskyy, A.V. Lyulin, A.R.C. Baljon, N.K. Balabaev, M.A.J. Michels, 'Effects of Strong Confinement on the Glass-Transition Temperature in Simulated Atactic Polystyrene Films', *Macromolecules*, **44**, 2299–2310 2011.

113. J.D. Yeager, M. Dubey, M.J. Wolverton, M.S. Jablin, J. Majewski, D.F. Bahr, D.E. Hooks, 'Examining Chemical Structure at the Interface Between a Polymer Binder and a Pharmaceutical Crystal with Neutron Reflectometry', *Polymer*, **52**, 3762–3768 2011.

114. A. Vorobiev, J. Major, H. Dosch, P. Mueller-Buschbaum, P. Falus, G.P. Felcher, S.G.E. te Velthuis, 'Phase and Microphase Separation of Polymer Thin Films Dewetted from Silicon-A Spin-Echo Resolved Grazing Incidence Neutron Scattering Study', *J. Phys. Chem. B*, **115**, 5754–5765 2011.

115. L.A. Sasa, E.J. Yearley, C.F. Welch, M.A. Taylor, R.D. Gilbertson, C. Hammeter, J. Majewski, R.P. Hjelm, 'The Los Alamos Neutron Science Center Neutron Rheometer in the Cone and Plate Geometry to Examine Tethered Polymers/Polymer Melt Interfaces Via Neutron Reflectivity', *Rev. Sci. Instrum.*, **81**, 055102 2010.

116. A.R. Bras, R. Pasquino, T. Koukoulas, G. Tsolou, O. Holderer, A. Radulescu, J. Allgaier, V.G. Mavrantzas, W. Pyckhout-Hintzen, A. Wischnewski, Ds. Vlassopoulos, D. Richter, 'Structure and Dynamics of Polymer Rings by Neutron Scattering: Breakdown of the Rouse Model', *Soft Matter*, **7**, 11169–11176 2011.

117. A. Arbe, J. Colmenero, 'Characterization of the ''Simple-Liquid'' State in a Polymeric System: Coherent and Incoherent Scattering Functions', *Phys. Rev. E*, **80**, 041805 2009.

118. X. Frielinghaus, M. Brodeck, Ol. Holderer, H. Frielinghaus, 'Confined Polymer Dynamics on Clay Platelets', *Langmuir*, **26**, 17444–17448 2010.

119. J.E. Martin, 'Configurational Diffusion in Semidilute Solutions', *Macromolecules*, **19**, 1281–1284 1986.

FURTHER READING

V. Arrighi, J.S. Higgins, 'Structural Investigation of Polymers by Neutron Scattering', *Plast. Rubber. Compos.*, **33**, 313–329 2004.

D.G. Bucknall and V. Arrighi, ''Neutron Scattering and Polymer Blends'', in *Polymer Blends*, eds. D.R. Paul and C.B. Bucknall, Wiley, Chapter 12, 1999.

J.P. Embs, J. Fanni, R. Hempelmann, 'Introduction to Quasielastic Neutron Scattering', *Z. Phys. Chem. Int. J. Res. Phys. Chem. Chem. Phys.*, **224**, 5–32 2010.

M.R. Fitzsimmons, S.D. Bader, J.A. Borchers, G.P. Felcher, J.K. Furdyna, A. Hoffmann, J.B. Kortright, Ivan.K. Schuller, T.C. Schulthess, S.K. Sinha, M.F. Toney, D. Weller, S. Wolf, 'Neutron Scattering Studies of Nanomagnetism and Artificially Structured Materials', *J. Magn. Magn. Mater.*, **271**, 103–146 2004.

A. Furrer, J. Mesot, T. Strässle, *Neutron Scattering in Condensed Matter Physics*, World Scientific Publ., 2009.

B. Hammouda, 'SANS from Polymers – Review of the Recent Literature', *Macromol. Sci. C, Polym. Rev.*, **50**, 14–39 2010.

T. Hashimoto, 'Small-Angle Neutron Scattering Studies of Dynamics and Hierarchical Pattern Formation in Binary Mixtures of Polymers and Small Molecules', *J. Polym. Sci., Polym. Phys. Ed.*, **42**, 3027–3062 2004.

T. Kanaya, K. Kaji, 'Dynamics in the Glassy State and Near the Glass Transition of Amorphous Polymers as Studied by Neutron Scattering', *Polym. Phys. Eng. Adv. Polym. Sci.*, **154**, 87–141 2001.

Y.B. Melnichenko, G.D. Wignall, 'Small-Angle Neutron Scattering in Materials Science: Recent Practical Applications', *J. Appl. Phys.*, **102**, 021101 2007.

M. Monkenbusch, D. Richter, 'High Resolution Neutron Spectroscopy - ATool for the Investigation of Dynamics of Polymers and Soft Matter', *C. R. Phys.*, **8**, 845–864 2007.

K. Mortensen, ''Structural Studies of Polymer Systems Using Small-Angle Neutron Scattering'', in *Advanced Functional Molecules and Polymers, Processing and Spectroscopy*, eds. H.S. Nalwa, Overseas Publ. Assoc., Oxford, UK Vol. 2, Chapter 8, 2001.

I. Olivier, 'A Review of In Situ and/Or Time Resolved Neutron Scattering', *C. R. Phys.*, **8**, 789–805 2007.

D. Richter, 'Neutron Scattering in Polymer Physics', *Physica B*, **276**, 22–29 2000.

D. Richter, D.A. Neumann, 'Neutron Scattering Studies of Dynamics: A New Frontier in Materials Science', *MRS Bull.*, **28**, 913–917 2003.

R.J. Roe, *Methods of X-ray and Neutron Scattering in Polymer Science*, Oxford Univ. Press, Oxford, UK 2000.

S.E. Rogers, A.E. Terry, M.J. Lawrence, J. Eastoe, J.T. Cabral, A. Chan, 'Soft Matter at ISIS', *Mater. Today*, **12**, 92–99 2009.

P. Thiyagarajan, 'Characterization of Materials of Industrial Importance Using Small-Angle Scattering Techniques', *J. Appl. Cryst.*, **36**, 373–380 2003.

G.D. Wignall, Y.B. Melnichenko, 'Recent Applications of Small-Angle Neutron Scattering in Strongly Interacting Soft Condensed Matter', *Rep. Prog. Phys.*, **68**, 1761–1810 2005.

B.T.M. Willis, C.J. Carlile, *Experimental Neutron Scattering*, Oxford University Press, Oxford, UK 2009.

Encyclopedia of Analytical Chemistry, Online © 2006–2012 John Wiley & Sons, Ltd.
This article is © 2012 John Wiley & Sons, Ltd.
This article was published in the *Encyclopedia of Analytical Chemistry* in 2012 by John Wiley & Sons, Ltd.
DOI: 10.1002/9780470027318.a2022.pub2